

# Achieving Shrinkage in a Time-Varying Parameter Model Framework

Angela Bitto and Sylvia Frühwirth-Schnatter\*

June 5, 2018

## Abstract

Shrinkage for time-varying parameter (TVP) models is investigated within a Bayesian framework, with the aim to automatically reduce time-varying parameters to static ones, if the model is overfitting. This is achieved through placing the double gamma shrinkage prior on the process variances. An efficient Markov chain Monte Carlo scheme is developed, exploiting boosting based on the ancillarity-sufficiency interweaving strategy. The method is applicable both to TVP models for univariate as well as multivariate time series. Applications include a TVP generalized Phillips curve for EU area inflation modelling and a multivariate TVP Cholesky stochastic volatility model for joint modelling of the returns from the DAX-30 index.

*Keywords:* Bayesian inference; Bayesian Lasso; double gamma prior; hierarchical priors; Kalman filter; log predictive density scores; normal-gamma prior; sparsity; state space model.

## 1 Introduction

Time-varying parameter (TVP) models are widely used in time series analysis to deal with processes which gradually change over time and provide an interesting alternative to models that allow multiple change points as considered, for instance, in Geweke and Jiang (2011). A variety of interesting econometric applications of TVP models appeared in recent years; for example, Primiceri (2005) used time-varying structural VAR models in a monetary policy application, Dangl and Halling (2012) used TVP models for equity return prediction and Belmonte et al. (2014) used a TVP model to model EU-area inflation.

---

\*Institute for Statistics and Mathematics, Department of Finance, Accounting and Statistics, WU Vienna University of Economics and Business, Vienna, Austria; email: angela.bitto@wu.ac.at and sfruehwi@wu.ac.at.

A huge advantage of TVP models is their flexibility in capturing gradual changes. However, the risk of overfitting increases with a growing number of coefficients, as many of them might in reality be constant over the entire observation period. This will be exemplified in the present paper for a TVP Cholesky stochastic volatility (SV) model (Lopes et al., 2016) for a time series of returns from the DAX-30 index, where out of 406 potentially time-varying coefficients only a small fraction actually changes over time. Allowing static coefficients to be time-varying leads to a considerable loss of statistical efficiency compared to a model, where coefficients are constant apriori.

Identifying fixed coefficients in a TVP model amounts to a *variance selection* problem, involving a decision whether the variances of the shocks driving the dynamics of a time-varying parameter are equal to zero. Variance selection in latent variable models is known to be a non-regular problem within the framework of classical statistical hypothesis testing (Harvey, 1989). The introduction of shrinkage priors for variances within a Bayesian framework has proven to be an attractive alternative both for random effects models (Frühwirth-Schnatter and Tüchler, 2008; Frühwirth-Schnatter and Wagner, 2011) as well as state space models (Frühwirth-Schnatter, 2004; Frühwirth-Schnatter and Wagner, 2010; Nakajima and West, 2013; Belmonte et al., 2014; Kalli and Griffin, 2014). For TVP models, shrinkage priors can automatically reduce time-varying coefficients to static ones, if the model is overfitting.

The literature on variance selection in TVP models is still rather slender, despite this pioneering work, compared to the vast literature on *variable selection* using shrinkage priors to shrink coefficients toward zero in a common regression framework. This class includes mixture priors such as spike-and-slab priors which assign positive probability to zero values (Mitchell and Beauchamp, 1988) and stochastic search variable selection (SSVS) priors (George and McCulloch, 1993) as well as continuous shrinkage priors with a pronounced spike at zero, well-known examples being the Bayesian Lasso prior (Park and Casella, 2008), the normal-gamma prior (Griffin and Brown, 2010; Caron and Doucet, 2008) and the horseshoe prior (Carvalho et al., 2010), among many others; see Fahrmeir et al. (2010) and Polson and Scott (2011) for a review.

One of the main contributions of Frühwirth-Schnatter and Wagner (2010) has been to recast the *variance selection* problem for state space models as a *variable selection* problem in the so-called non-centered parametrization of the state space model. This established the possibility to extend shrinkage priors from standard regression analysis to this more general framework to define a “sparse” state space model. To this aim, Frühwirth-Schnatter and Wagner (2010) employed spike-and-slab priors, whereas Belmonte et al. (2014) relied on the Bayesian Lasso prior for variance selection in TVP models. However, other shrinkage priors might be useful and overcome limitations of these priors, such as

computational issues for the spike-and-slab prior and the risk of overshrinking coefficients for the Bayesian Lasso prior.

The present paper makes several contributions in the context of sparse state space models. We develop a new continuous shrinkage prior for process variances by introducing the normal-gamma prior in the non-centered parametrization. This leads to a gamma-gamma (called double gamma) prior for the process variances, which has many attractive properties compared to the popular inverted gamma prior (Petrakis et al., 2009). We show that the double gamma prior is more flexible than the Bayesian Lasso prior (which is a special case of the double gamma) and yields posterior distributions with a pronounced spike at zero for coefficients which are not time-varying, while at the same time overshrinkage is avoided for time-varying coefficients. A second shrinkage prior allows to shrink static coefficients to coefficients which are not significant over the entire observation period. As a result, we are able to discriminate between time-varying coefficients, coefficients which are significant, but static and insignificant coefficients. We compare different prior settings using log predictive density scores (Geweke and Amisano, 2010) and discuss an accurate approximation of the one-step ahead predictive density.

Based on these priors, we define a very general class of sparse TVP models, both for univariate and multivariate times series, and allow for homoscedastic error variances as well as error variances following a stochastic volatility (SV) model (Jacquier et al., 1994). The later model has proven to be useful in various applications, because neglecting time-varying volatilities might lead to overstating the role of time-varying coefficients in explaining structural changes in the dynamics of macroeconomic variables, as exemplified by Sims (2001) and Nakajima (2011).

Finally, we develop a new Markov chain Monte Carlo (MCMC) scheme for Bayesian inference in sparse TVP models. Using the scale-mixture representation of the normal-gamma prior allows us to implement full conditional Gibbs sampling, thus avoiding Metropolis-Hastings steps which are often used to implement MCMC methods for non-Gaussian state space models, see e.g. Geweke and Tanizaki (1999). To improve MCMC performance, we exploit the ancillarity-sufficiency interweaving strategy of Yu and Meng (2011).

The rest of the paper is structured as follows. Section 2 discusses our novel shrinkage method in the context of sparse TVP models. In Section 3, we present the MCMC scheme. Section 4 discusses evaluation of various priors using log predictive density scores. In Section 5, we extend our method to a multivariate framework. Section 6 presents a simulated data example and Section 7 exemplifies our approach through EU area inflation modelling based on the generalized Phillips curve as well as estimating a time-varying covariance matrix based on a TVP Cholesky SV model for a multivariate time series of returns of the DAX-30 index. Section 8 concludes.

## 2 Sparse time-varying parameter models

### 2.1 Bayesian inference for time-varying parameter models

Starting point is the well known state space model, which has been studied in many fields, see e.g. West and Harrison (1997) for a comprehensive review. For the ease of exposition, we consider in this section a univariate time series  $y_t$ , observed for  $T$  time points  $t = 1, \dots, T$ , whereas multivariate time series are discussed in Section 5. In a state space model, the distribution of  $y_t$  is driven by a latent  $d$ -dimensional state vector  $\boldsymbol{\beta}_t$  which we are unable to observe. The time-varying parameter (TVP) model is a special case of a state space model and can be regarded as a regression model with time-varying regression coefficients  $\boldsymbol{\beta}_t$  following a random walk:

$$\boldsymbol{\beta}_t = \boldsymbol{\beta}_{t-1} + \boldsymbol{\omega}_t, \quad \boldsymbol{\omega}_t \sim \mathcal{N}_d(\mathbf{0}, \mathbf{Q}), \quad (1)$$

$$y_t = \mathbf{x}_t \boldsymbol{\beta}_t + \varepsilon_t, \quad \varepsilon_t \sim \mathcal{N}(0, \sigma_t^2), \quad (2)$$

where  $\mathbf{x}_t = (x_{t1}, x_{t2}, \dots, x_{td})$  is a  $d$ -dimensional row vector, containing the regressors of the model, one of them being a constant (e.g.  $x_{t1} \equiv 1$ ). To avoid any scaling issues, we assume that all covariates except the intercept are standardized such that for each  $j$  the average of  $x_{tj}$  over  $t$  is equal to zero and the sample variance is equal to 1. The unknown initial value  $\boldsymbol{\beta}_0$  is assumed to follow a normal prior distribution,

$$\boldsymbol{\beta}_0 | \boldsymbol{\beta}, \mathbf{Q} \sim \mathcal{N}_d(\boldsymbol{\beta}, \mathbf{P}_0 \mathbf{Q}), \quad (3)$$

with  $\boldsymbol{\beta} = (\beta_1, \dots, \beta_d)'$  being unknown fixed regression coefficients and  $\mathbf{P}_0 = \text{Diag}(P_{0,11}, \dots, P_{0,dd})$  being a diagonal matrix. Furthermore,  $\boldsymbol{\beta}_0$  is independent of the innovations  $(\varepsilon_t)$  and  $(\boldsymbol{\omega}_t)$ , which are independent Gaussian white noise processes.

We assume that  $\mathbf{Q} = \text{Diag}(\theta_1, \dots, \theta_d)$  is a diagonal matrix, hence each element  $\beta_{jt}$  of  $\boldsymbol{\beta}_t = (\beta_{1t}, \dots, \beta_{dt})'$  follows a random walk for  $j = 1, \dots, d$ :

$$\beta_{jt} = \beta_{j,t-1} + \omega_{jt}, \quad \omega_{jt} \sim \mathcal{N}(0, \theta_j), \quad (4)$$

with initial value  $\beta_{j0} | \beta_j, \theta_j, P_{0,jj} \sim \mathcal{N}(\beta_j, \theta_j P_{0,jj})$ . Hence,  $\theta_j$  is the process variance governing the dynamics of the time-varying coefficient  $\beta_{jt}$ .<sup>1</sup>

Concerning the error variances in the observation equation (2), we consider the homoscedastic case ( $\sigma_t^2 \equiv \sigma^2$  for all  $t = 1, \dots, T$ ) as well as a more flexible model specification, where  $\sigma_t^2$  is time-dependent. To capture heteroscedasticity, we use a stochastic

---

<sup>1</sup>Eisenstat et al. (2014) discuss an extension where the covariance matrix  $\mathbf{Q}$  in the state equation (1) is a full matrix instead of a diagonal matrix.

volatility (SV) specification as in Jacquier et al. (1994) where  $\sigma_t^2 = e^{h_t}$  and the log volatility  $h_t$  follows an AR(1) process:

$$h_t | h_{t-1}, \mu, \phi, \sigma_\eta^2 \sim \mathcal{N}(\mu + \phi(h_{t-1} - \mu), \sigma_\eta^2). \quad (5)$$

In this setup, the latent volatility process  $\mathbf{h} = (h_0, \dots, h_T)$  is not observed and the initial state  $h_0$  is assumed to follow the stationary distribution of the autoregressive process, i.e.  $h_0 | \mu, \phi, \sigma_\eta^2 \sim \mathcal{N}(\mu, \sigma_\eta^2 / (1 - \phi^2))$ .

We perform Bayesian inference for the TVP model based on a new family of shrinkage priors for the unknown model parameters  $\boldsymbol{\beta} = (\beta_1, \dots, \beta_d)'$  and  $\boldsymbol{\theta} = (\theta_1, \dots, \theta_d)'$  to be introduced in Section 2.2. A shrinkage prior for the process variance  $\theta_j$  allows to pull the  $j$ th time-varying regression coefficient  $\{\beta_{j0}, \beta_{j1}, \dots, \beta_{jT}\}$  toward the fixed regression coefficient  $\beta_j$ , if the model is overfitting and the effect of the  $j$ th covariate  $x_{tj}$  is, in fact, not changing over time. This requires the definition of priors on the process variances  $\theta_j$  that are able to shrink  $\theta_j$  toward the boundary value 0. At the same time, these priors are flexible enough to avoid overshrinking for regression coefficients that are, actually, changing over time  $t$  and are characterized by a non-zero process variance  $\theta_j \neq 0$ .

Concerning the remaining priors, we assume that the scaling factor  $P_{0,jj}$  in the initial distribution  $\beta_{j0} | \beta_j, \theta_j, P_{0,jj} \sim \mathcal{N}(\beta_j, \theta_j P_{0,jj})$  is unknown, following the prior  $P_{0,jj} \sim \mathcal{G}^{-1}(\nu_P, (\nu_P - 1)c_P)$  with hyperparameters  $c_P = 1$  and  $\nu_P = 20$ , implying that no prior moments exist. We employ commonly used priors for the parameters of the error distribution in the equation (1), namely a hierarchical prior for the homoscedastic case,

$$\sigma^2 | C_0 \sim \mathcal{G}^{-1}(c_0, C_0), \quad C_0 \sim \mathcal{G}(g_0, G_0), \quad (6)$$

with hyperparameters  $c_0$ ,  $g_0$ , and  $G_0$ . In our practical applications,  $c_0 = 2.5$ ,  $g_0 = 5$ , and  $G_0 = g_0 / E(\sigma^2)(c_0 - 1)$ , with  $E(\sigma^2)$  being a prior guess of  $\sigma^2$ .

In the SV framework (5), unknown parameters are the level  $\mu$ , the persistence  $\phi$ , and the volatility of volatility  $\sigma_\eta^2$ . The priors are chosen as in Kastner and Frühwirth-Schnatter (2014), assuming prior independence, i.e.  $p(\mu, \phi, \sigma_\eta^2) = p(\mu)p(\phi)p(\sigma_\eta^2)$ , with  $\mu \sim \mathcal{N}(b_\mu, B_\mu)$ ,  $(\phi + 1)/2 \sim \mathcal{B}(a_0, b_0)$ , and  $\sigma_\eta^2 \sim \mathcal{G}(\frac{1}{2}, \frac{1}{2B_\sigma})$ , with hyperparameters  $b_\mu = 0$ ,  $B_\mu = 100$ ,  $a_0 = 20$ ,  $b_0 = 1.5$ , and  $B_\sigma = 1$ .

An important building block of our approach is a non-centered parametrization of the TVP model in the vein of Frühwirth-Schnatter and Wagner (2010). First, we define  $d$  independent random walk processes  $\tilde{\beta}_{jt}, j = 1, \dots, d$ , with standard normal independent increments, i.e.

$$\tilde{\beta}_{jt} = \tilde{\beta}_{j,t-1} + \tilde{\omega}_{jt}, \quad \tilde{\omega}_{jt} \sim \mathcal{N}(0, 1), \quad (7)$$

and initial value  $\tilde{\beta}_{j0}|P_{0,jj} \sim \mathcal{N}(0, P_{0,jj})$ . Using the transformation

$$\beta_{jt} = \beta_j + \sqrt{\theta_j} \tilde{\beta}_{jt}, \quad t = 0, \dots, T, \quad (8)$$

we rewrite the state space model (2) and (4) by combining the  $d$  state equations for  $\tilde{\beta}_{jt}$  given in (7) with following observation equation:

$$y_t = \mathbf{x}_t \boldsymbol{\beta} + \mathbf{x}_t \text{Diag}(\sqrt{\theta_1}, \dots, \sqrt{\theta_d}) \tilde{\boldsymbol{\beta}}_t + \varepsilon_t. \quad (9)$$

The resulting state space model with state vector  $\tilde{\boldsymbol{\beta}}_t = (\tilde{\beta}_{1t}, \dots, \tilde{\beta}_{dt})'$  is an alternative parametrization of the TVP model, where the observation equation (9) contains all unknown parameters, i.e. the fixed regression coefficients  $\beta_1, \dots, \beta_d$ , as well as the (square roots of the) unknown process variances  $\theta_1, \dots, \theta_d$ , whereas the state equations (7) are independent of any parameter. Such a parameterization is called non-centered in the spirit of Papaspiliopoulos et al. (2007), whereas the original parametrization (2) and (4) is called centered. Note that the initial state in the non-centered parametrization follows  $\tilde{\boldsymbol{\beta}}_0|\mathbf{P}_0 \sim \mathcal{N}_d(0, \mathbf{P}_0)$  with  $\mathbf{P}_0 = \text{Diag}(P_{0,11}, \dots, P_{0,dd})$ .

## 2.2 Shrinking process variances through the double gamma prior

A popular prior choice for the process variance  $\theta_j$  is the inverted gamma distribution, which is the conjugate prior for  $\theta_j$  in the centered parameterization (4), see e.g. Petris et al. (2009):

$$\theta_j \sim \mathcal{G}^{-1}(s_0, S_0). \quad (10)$$

However, as shown by Frühwirth-Schnatter and Wagner (2010), this prior fails to introduce shrinkage as it is bounded away from zero. Frühwirth-Schnatter (2004) introduced a shrinkage prior for the process variance in a univariate TVP model (that is  $d = 1$ ) through the scale parameter in the non-centered parametrization (9) and Frühwirth-Schnatter and Wagner (2010) extended this idea to state space models with  $d > 1$ . The scale parameter  $\sqrt{\theta_j} \in \mathbb{R}$  is defined as the positive and the negative root of  $\theta_j$  and is allowed to take on positive and negative values. Since the conjugate prior for  $\sqrt{\theta_j}$  in the non-centered parameterization (9) is the normal distribution,  $\sqrt{\theta_j}$  is assumed to be Gaussian with zero mean and scale parameters  $\xi_j^2$ :

$$\sqrt{\theta_j}|\xi_j^2 \sim \mathcal{N}(0, \xi_j^2) \quad \Leftrightarrow \quad \theta_j|\xi_j^2 \sim \mathcal{G}\left(\frac{1}{2}, \frac{1}{2\xi_j^2}\right). \quad (11)$$

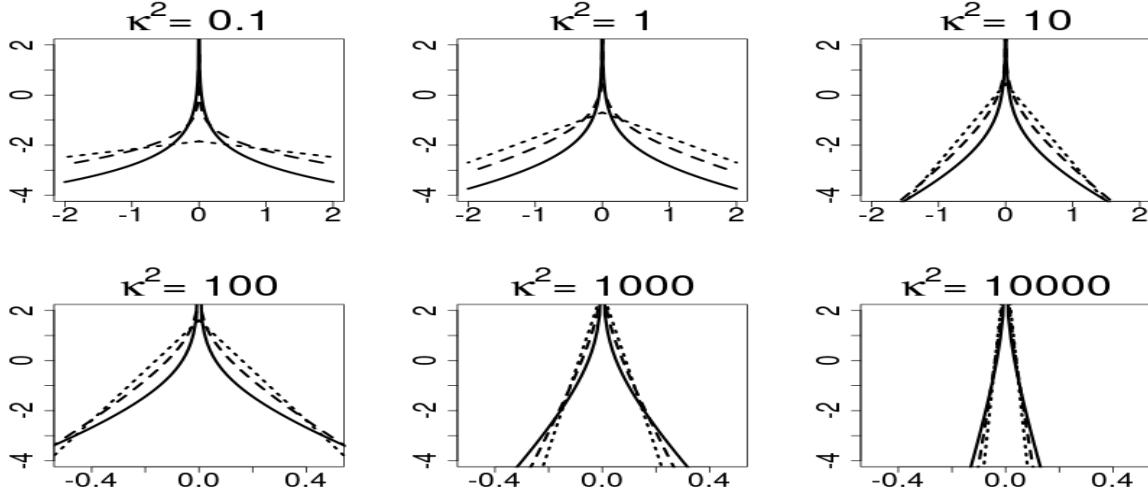


Figure 1:  $\text{Log } p(\sqrt{\theta_j}|a^\xi, \kappa^2)$  of the double gamma prior for different values of  $\kappa^2$  and  $a^\xi = 0.1$  (solid line),  $a^\xi = 1/3$  (dashed line) and  $a^\xi = 1$  (dotted line).

Shrinking  $\theta_j$  toward the boundary value is achieved by shrinking  $\sqrt{\theta_j}$  toward 0 (which is an interior point of the parameter space in the non-centered parametrization). For a sparse state space model, prior (11) substitutes the inverted gamma prior (10) by a gamma prior.<sup>2</sup>

To discriminate between static and time-varying components, Frühwirth-Schnatter and Wagner (2010) introduced spike-and-slab priors, where  $\xi_j^2 = 0$  with positive prior probability and  $\xi_j^2$  is fixed, otherwise (e.g.  $\xi_j^2 = 10$ ). Instead of using spike-and-slab priors, Belmonte et al. (2014) extended prior (11) by adding two levels of hierarchy to define a hierarchical Bayesian Lasso prior, where  $\xi_j^2$  follows an exponential distribution.

In the present paper, we introduce a more general family of shrinkage priors derived from the normal-gamma prior, introduced by Griffin and Brown (2010) for variable selection in standard regression models and applied in Caron and Doucet (2008) to multivariate regression models. The main idea is to use the normal-gamma prior as a prior for  $\sqrt{\theta_j}$  in the non-centered state space model, extending (11). The normal-gamma prior is a scale mixture of normal distributions with following hierarchical representation:

$$\sqrt{\theta_j}|\xi_j^2 \sim \mathcal{N}(0, \xi_j^2), \quad \xi_j^2|a^\xi, \kappa^2 \sim \mathcal{G}(a^\xi, a^\xi \kappa^2/2). \quad (12)$$

In terms of the process variances  $\theta_j$ , (12) implies that  $\theta_j$  follows a “double gamma” prior:

$$\theta_j|\xi_j^2 \sim \mathcal{G}\left(\frac{1}{2}, \frac{1}{2\xi_j^2}\right), \quad \xi_j^2|a^\xi, \kappa^2 \sim \mathcal{G}(a^\xi, a^\xi \kappa^2/2). \quad (13)$$

<sup>2</sup>We use the parametrization of the  $\mathcal{G}(\alpha, \beta)$  distribution with pdf given by  $f(y) = \beta^\alpha y^{\alpha-1} e^{-\beta y} / \Gamma(\alpha)$ .

For  $a^\xi = 1$ ,  $\xi_j^2|a^\xi, \kappa^2$  reduces to an exponential distribution and the Bayesian Lasso prior considered by Belmonte et al. (2014) results as a special case of the double gamma prior. Marginalizing over  $\xi_j^2$  yields closed form expressions for  $p(\sqrt{\theta_j}|a^\xi, \kappa^2)$  and  $p(\theta_j|a^\xi, \kappa^2)$ :<sup>3</sup>

$$\begin{aligned} p(\sqrt{\theta_j}|a^\xi, \kappa^2) &= \frac{(\sqrt{a^\xi \kappa^2})^{a^\xi+1/2}}{\sqrt{\pi} 2^{a^\xi-1/2} \Gamma(a^\xi)} |\sqrt{\theta_j}|^{a^\xi-1/2} K_{a^\xi-1/2}(\sqrt{a^\xi \kappa^2} |\sqrt{\theta_j}|), \\ p(\theta_j|a^\xi, \kappa^2) &= \frac{(\sqrt{a^\xi \kappa^2})^{a^\xi+1/2}}{\sqrt{\pi} 2^{a^\xi-1/2} \Gamma(a^\xi)} (\theta_j)^{a^\xi/2-3/4} K_{a^\xi-1/2}(\sqrt{a^\xi \kappa^2 \theta_j}), \end{aligned} \quad (14)$$

where  $K_p(\cdot)$  is the modified Bessel function of the second kind with index  $p$ . The display of  $\log p(\sqrt{\theta_j}|a^\xi, \kappa^2)$  for different values of  $\kappa^2$  in Figure 1 shows that the double gamma prior with  $a^\xi \leq 1$  is an example of a global-local shrinkage prior (Polson and Scott, 2011). A pronounced spike at zero is present and the mass placed close to zero strongly depends on the global parameter  $\kappa^2$ . From representation (13) we obtain that, marginally,  $E(\theta_j) = 2/\kappa^2$ , whereas

$$V(\theta_j) = E(\theta_j^2) - E(\theta_j)^2 = 3E((\xi_j^2)^2) - \frac{4}{\kappa^4} = \frac{12}{a^\xi \kappa^4} + \frac{8}{\kappa^4} = E(\theta_j)^2 (2 + 3/a^\xi).$$

Hence, independently of  $a^\xi$ , the hyperparameter  $\kappa^2$  controls the global level of shrinkage, which is the stronger, the larger  $\kappa^2$ . At the same time, also  $V(\theta_j)$  decreases, as  $\kappa$  increases. Therefore, the larger  $\kappa^2$ , the more mass is placed close to zero. On the other hand, the term  $3/a^\xi$  – which is equal to the excess kurtosis of  $\sqrt{\theta_j}$  – controls local adaption to the global level of shrinkage, with more local adaption, the smaller  $a^\xi$ . As  $a^\xi$  decreases, the excess kurtosis of  $\sqrt{\theta_j}$  increases and the tails of  $p(\sqrt{\theta_j}|a^\xi, \kappa^2)$  become thicker.

It is also illuminating to investigate the joint marginal prior distribution of  $(\theta_1, \dots, \theta_d)$  or (equivalently) of  $(\sqrt{\theta_1}, \dots, \sqrt{\theta_d})$  given  $a^\xi$  and  $\kappa^2$ . Since the random prior variances  $\xi_j^2$  in (13) are drawn independently, also marginally the double gamma prior is characterized by prior conditional independence of  $(\theta_1, \dots, \theta_d)$  given fixed values of  $a^\xi$  and  $\kappa^2$ :  $p(\theta_1, \dots, \theta_d|a^\xi, \kappa^2) = \prod_{j=1}^d p(\theta_j|a^\xi, \kappa^2)$ .

For illustration, Figure 2 shows simulations from the joint prior  $p(\sqrt{\theta_1}, \sqrt{\theta_2}|a^\xi, \kappa^2)$  for  $d = 2$  for various values of  $a^\xi$  and  $\kappa^2$ . Not surprisingly from the previous discussions, for the same value of  $\kappa^2$ , the double gamma with  $a^\xi = 0.1$  has a pronounced spike at 0 with fat tails in both directions of  $\sqrt{\theta_1}$  and  $\sqrt{\theta_2}$  and provides more flexible shrinkage compared to the Bayesian Lasso prior ( $a^\xi = 1$ ). For the Bayesian Lasso prior, large values of  $\kappa^2$  (e.g.  $\kappa^2 = 200$ ) are needed to introduce strong shrinkage toward 0.

To infer appropriate values of  $a^\xi$  and  $\kappa^2$  from the data, hierarchical priors are employed.

---

<sup>3</sup>Note that  $F_{\theta_j}(c) = \Pr(\theta_j \leq c) = \Pr(-\sqrt{c} \leq \sqrt{\theta_j} \leq \sqrt{c}) = 2F_{\sqrt{\theta_j}}(\sqrt{c})$ , where  $F_{\theta_j}(\cdot)$  is the cdf of the random variable  $\sqrt{\theta_j}$ . Therefore,  $p(\theta_j|a^\xi, \kappa^2) = p(\sqrt{\theta_j}|a^\xi, \kappa^2)/\sqrt{\theta_j}$ .



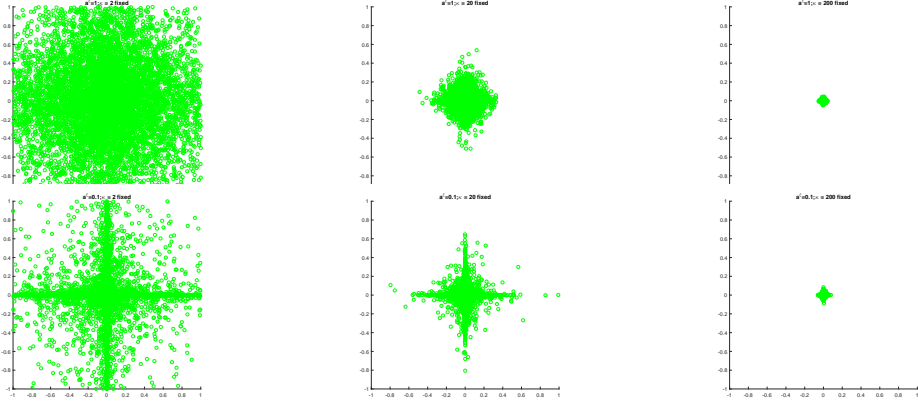


Figure 2: Simulations from the double gamma prior  $p(\sqrt{\theta_1}, \sqrt{\theta_2} | a^\xi, \kappa^2)$  for  $a^\xi = 1$  (top) and  $a^\xi = 0.1$  (bottom) for different values of  $\kappa^2$  (left-hand side:  $\kappa^2 = 2$ , middle:  $\kappa^2 = 20$ , right-hand side:  $\kappa^2 = 200$ ). The plots at the top correspond to the Bayesian Lasso prior.

We assume that  $\kappa^2$  follows a gamma distribution with fixed hyperparameters  $d_1$  and  $d_2$ :

$$\kappa^2 \sim \mathcal{G}(d_1, d_2). \quad (15)$$

For  $a^\xi = 1$  this corresponds to the hierarchical Bayesian Lasso prior considered by Belmonte et al. (2014). In addition, we assume that the shrinkage parameter  $a^\xi$  follows an exponential distribution as in Griffin and Brown (2010),

$$a^\xi \sim \mathcal{E}(b^\xi), \quad (16)$$

with a fixed hyperparameter  $b^\xi \geq 1$ . Combining (13) with (15) and (16) defines the hierarchical double gamma prior. Given the hyperparameters  $d_1$ ,  $d_2$ , and  $b^\xi$ , this hierarchical prior introduces prior dependence among  $(\theta_1, \dots, \theta_d)$  which is advantageous in a shrinkage framework, as recently shown by Griffin and Brown (2017). Prior dependence is desirable in situations, where only a few variances are expected to be different from 0. In this case, whether a certain process variance is shrunk toward 0 depends on how close the other process variances are to 0.

Prior dependence also exists between  $\beta_{j0}$  and  $\theta_j$ , as the size (but not the sign) of  $\beta_{j0} - \beta_j$  depends on  $\theta_j$  through  $V(\beta_{j0} - \beta_j | \theta_j) = \theta_j P_{0,jj}$ . If  $\theta_j$  is shrunk toward 0, then  $\beta_{j0}$  and all subsequent values  $\beta_{jt}$  are pulled toward  $\beta_j$  for covariate  $x_{tj}$ . In high dimensions, where many coefficients are expected to be static, it is of interest to allow a practically constant coefficient  $\beta_{jt}$  to be insignificant throughout the entire observation period. As these coefficients are characterized by a parameter setting where both  $\theta_j$  and  $\beta_j$  are close to 0, a second normal-gamma prior is employed as a shrinkage prior for  $\beta_j$  to allow shrinkage

of  $\beta_j$  toward 0:<sup>4</sup>

$$\beta_j | \tau_j^2 \sim \mathcal{N}(0, \tau_j^2), \quad \tau_j^2 | a^\tau, \lambda^2 \sim \mathcal{G}(a^\tau, a^\tau \lambda^2 / 2). \quad (17)$$

In this case, any (practically constant) coefficient  $\beta_{jt}$  is insignificant, whenever the corresponding fixed regression effect  $\beta_j$  is zero.<sup>5</sup> Similarly as for  $\theta_j$ , another layer of hierarchy is added, by assuming that  $\lambda^2 \sim \mathcal{G}(e_1, e_2)$  and  $a^\tau \sim \mathcal{E}(b^\tau)$  with fixed hyperparameters  $e_1, e_2$  and  $b^\tau \geq 1$ .

### 3 MCMC Estimation

To carry out Bayesian inference for a sparse TVP model under the shrinkage priors introduced in Section 2, we develop an efficient scheme for Markov chain Monte Carlo (MCMC) sampling, given all hyperparameters, i.e.  $e_1, e_2, b^\tau, d_1, d_2, b^\xi$  in the priors for  $\boldsymbol{\beta}$  and  $\mathbf{Q}$ ,  $c_P, \nu_P$  in the prior of  $P_{0,11}, \dots, P_{0,dd}$ , as well as  $c_0, g_0, G_0$  for homoscedastic variances  $\sigma^2$  and  $b_\mu, B_\mu, a_0, b_0, B_\sigma$  for parameters of the SV model (5). Bayesian inference operates in the latent variable formulation of the TVP model and relies on data augmentation of the latent processes  $\boldsymbol{\beta} = (\boldsymbol{\beta}_0, \boldsymbol{\beta}_1, \dots, \boldsymbol{\beta}_T)$  for the centered and  $\tilde{\boldsymbol{\beta}} = (\tilde{\boldsymbol{\beta}}_0, \tilde{\boldsymbol{\beta}}_1, \dots, \tilde{\boldsymbol{\beta}}_T)$  for the non-centered parameterization. For the SV model, the log volatilities  $\mathbf{h} = (h_0, \dots, h_T)$  are introduced as additional latent variables.

For the centered parameterization under the common inverted gamma prior (10) for the process variances  $\theta_j$ , Gibbs sampling is totally standard, see e.g. Petris et al. (2009). However, if some of the process variances are small, then this MCMC scheme suffers from slow convergence and poor mixing of the sampler. As shown by Frühwirth-Schnatter and Wagner (2010), MCMC estimation based on the non-centered parameterization proves to be useful, in particular if process variances are close to 0.

Frühwirth-Schnatter (2004) discusses the relationship between the various parametrizations for a simple TVP model and the computational efficiency of the resulting MCMC samplers, see also Papaspiliopoulos et al. (2007). For TVP models with  $d > 1$ , MCMC estimation in the centered parameterization is preferable for all coefficients that are actually time-varying, whereas the non-centered parametrization is preferable for (nearly) constant coefficients. For practical time series analysis, both types of coefficients are likely to be present and choosing a computationally efficient parametrization in advance is not possible.

---

<sup>4</sup>A closed form expression, comparable to (14), is available for  $p(\beta_j | a^\tau, \lambda^2)$ , with expectation  $E(|\beta_j|) = \sqrt{\frac{4}{\pi a^\tau \lambda^2}} \frac{\Gamma(a^\tau + 1/2)}{\Gamma(a^\tau)}$ ,  $V(\beta_j) = \frac{2}{\lambda^2}$ , while the excess kurtosis is given by  $\frac{3}{a^\tau}$ .

<sup>5</sup>It should be noted that the data are not informative about  $\beta_j$ , if  $\theta_j > 0$ , but they are always informative about the initial regression coefficient  $\beta_{j0}$ . For  $\theta_j = 0$ ,  $\beta_{j0}$  and  $\beta_j$  coincide.

We show how these two data augmentation schemes can be combined through the *ancillarity-sufficiency interweaving strategy* (ASIS) introduced by Yu and Meng (2011) to obtain an efficient sampler combining the “best of both worlds”. ASIS provides a principled way of interweaving different data augmentation schemes by re-sampling certain parameters conditional on the latent variables in the alternative parameterization of the model. This strategy has been successfully employed to univariate SV models (Kastner and Frühwirth-Schnatter, 2014), multivariate factor SV models (Kastner et al., 2017) and dynamic linear state space models (Simpson et al., 2017). In the present paper, ASIS is applied to interweave the centered and the non-centered parameterization of a TVP model. More specifically, we use the non-centered parametrization as baseline, and interweave into the centered parameterization. This leads to the MCMC sampling scheme outlined in Algorithm 1 which increases posterior sampling efficiency considerably compared to conventional Gibbs sampling for either of the two parameterizations.

**Algorithm 1.** Choose starting values for  $\beta, \mathbf{Q}, \tau = (\tau_1, \dots, \tau_d), \xi = (\xi_1, \dots, \xi_d), a^\tau, \lambda^2, a^\xi, \kappa^2, \mathbf{P}_0$ , and (for homoscedastic variances)  $\sigma^2$  and  $C_0$  and repeat the following steps:

- (a) Sample the states  $\tilde{\beta} = (\tilde{\beta}_0, \dots, \tilde{\beta}_T)$  in the non-centered parametrization from the multivariate Gaussian posterior  $\tilde{\beta}|\beta, \mathbf{Q}, \mathbf{P}_0, \sigma^2 \sim \mathcal{N}_{(T+1)d}(\Omega^{-1}\mathbf{c}, \Omega^{-1})$  given in (A.1).
- (b) Joint sampling of  $\alpha = (\beta_1, \dots, \beta_d, \sqrt{\theta_1}, \dots, \sqrt{\theta_d})'$  from the multivariate Gaussian posterior  $p(\alpha|\tilde{\beta}, \tau, \xi, \sigma^2, \mathbf{y})$  given in (A.3).
- (c) For each  $j = 1, \dots, d$ , redraw the constant coefficient  $\beta_j$  and the square root of the process variance  $\sqrt{\theta_j}$  through interweaving into the state equation of the centered parameterization:
  - (c-1) Use the transformation (8) to match the draws of the latent process  $\tilde{\beta}_{j0}, \dots, \tilde{\beta}_{jT}$  in the non-centered to the latent process  $\beta_{j0}, \dots, \beta_{jT}$  in the centered parameterization and store the sign of  $\sqrt{\theta_j}$ .
  - (c-2) Update  $\beta_j$  and  $\theta_j$  in the centered parameterization by sampling  $\theta_j^{\text{new}}$  from the generalized inverse Gaussian posterior  $\theta_j|\beta_{j0}, \dots, \beta_{jT}, \beta_j, \xi_j^2, P_{0,jj}$ , given in (18), and  $\beta_j^{\text{new}}$  from the Gaussian posterior  $\beta_j|\beta_{j0}, \theta_j^{\text{new}}, \tau_j^2, P_{0,jj}$ , given in (19).
  - (c-3) Determine  $\sqrt{\theta_j^{\text{new}}}$  using the same sign as the old value  $\sqrt{\theta_j}$ . Based on  $\sqrt{\theta_j^{\text{new}}}$  and  $\beta_j^{\text{new}}$ , the state process  $\tilde{\beta}_{jt}$  in the non-centered parameterization is updated in a deterministic manner through the inverse of the transformation (8):

$$\tilde{\beta}_{jt}^{\text{new}} = (\beta_{jt} - \beta_j^{\text{new}})/\sqrt{\theta_j^{\text{new}}}, \quad t = 0, \dots, T.$$

- (d) Sample from  $a^\tau | \beta_1, \dots, \beta_d, \lambda^2$  and  $a^\xi | \sqrt{\theta_1}, \dots, \sqrt{\theta_d}, \kappa^2$  using a random walk Metropolis-Hastings (MH) step based on proposing  $\log a^{\tau, \text{new}} \sim \mathcal{N}(\log a^\tau, c_\tau^2)$  and  $\log a^{\xi, \text{new}} \sim \mathcal{N}(\log a^\xi, c_\xi^2)$ .
- (e) Sample the prior variances  $\tau_j | \beta_j, a^\tau, \lambda^2$  and  $\xi_j | \theta_j, a^\xi, \kappa^2$ , for  $j = 1, \dots, d$ , from conditionally independent generalized inverse Gaussian distributions given in (A.4) and (A.5), respectively, and update the hyperparameters  $\lambda^2 | a^\tau, \boldsymbol{\tau}$  and  $\kappa^2 | a^\xi, \boldsymbol{\xi}$  from the gamma distributions given in (A.6) and (A.7).
- (f) Sample  $\sigma^2 | \tilde{\boldsymbol{\beta}}, \boldsymbol{\alpha}, C_0, \mathbf{y}$  from the following inverted gamma distribution

$$\sigma^2 | \tilde{\boldsymbol{\beta}}, \boldsymbol{\alpha}, C_0, \mathbf{y} \sim \mathcal{G}^{-1} \left( c_0 + \frac{T}{2}, C_0 + \frac{1}{2} \sum_{t=1}^T (y_t - \mathbf{z}_t \boldsymbol{\alpha})^2 \right),$$

where  $\mathbf{z}_t$  is defined in (A.2), and sample  $C_0$  from  $C_0 | \sigma^2 \sim \mathcal{G}(g_0 + c_0, G_0 + \frac{1}{\sigma^2})$ .

- (g) Sample the scale parameters of the initial distribution for each  $j = 1, \dots, d$ , from  $P_{0,jj} | \tilde{\beta}_{j0} \sim \mathcal{G}^{-1} \left( \nu_P + \frac{1}{2}, (\nu_P - 1)c_P + \frac{1}{2}\tilde{\beta}_{j0}^2 \right)$ .

After discarding a certain amount of initial draws (the *burn-in*), the full conditional sampler iterating Steps (a) to (g) of Algorithm 1 yields draws from the joint posterior distribution  $p(\tilde{\boldsymbol{\beta}}, \beta_1, \dots, \beta_d, \sqrt{\theta_1}, \dots, \sqrt{\theta_d}, \boldsymbol{\tau}, \boldsymbol{\xi}, a^\tau, \lambda^2, a^\xi, \kappa^2, \mathbf{P}_0, \sigma^2, C_0, | \mathbf{y})$  under the hierarchical shrinkage priors outlined in Section 2.2.

In Step (a), we sample the latent states  $\tilde{\boldsymbol{\beta}} = (\tilde{\boldsymbol{\beta}}_0, \dots, \tilde{\boldsymbol{\beta}}_T)$  in the non-centered parametrization conditional on known parameters  $\boldsymbol{\beta}, \mathbf{Q}, \mathbf{P}_0$  and known error variances  $\sigma^2$ . As an alternative to the commonly used *Forward Filtering Backward Sampling* (Frühwirth-Schnatter, 1994; Carter and Kohn, 1994), we implemented a multi-move sampling algorithm in the spirit of McCausland et al. (2011) which allows to sample the entire state process  $\tilde{\boldsymbol{\beta}}$  *all without a loop* (AWOL; Kastner and Frühwirth-Schnatter (2014)). Full details are provided in Appendix A.1.1.1.

In Step (b), conditional on the latent states  $\tilde{\boldsymbol{\beta}}$ , a regression type model results from the observation equation (9) of the non-centered state space model. Based on the Gaussian priors appearing in the hierarchical representations of the shrinkage priors (12) and (17), we sample the parameters  $\beta_1, \dots, \beta_d$  and  $\sqrt{\theta_1}, \dots, \sqrt{\theta_d}$  jointly from the conditionally Gaussian posterior given in (A.3); see Appendix A.1.1.2 for details. One major advantage of working with the square root of the process variance  $\sqrt{\theta_j}$ , instead of  $\theta_j$ , is that we avoid boundary space problems for small variances, resulting in better mixing behaviour of the sampler.

The interweaving Step (c) turns out to be instrumental for an efficient implementation of the hierarchical shrinkage priors introduced in Section 2.2. In this step, we temporarily

move from the non-centered to the centered parameterization to resample  $\beta_j$  and  $\theta_j$ . To ensure that the posterior distributions obtained with and without interweaving are identical, the priors between the non-centered and the centered parametrization are matched. Whereas the Gaussian prior  $\beta_j|\tau_j^2$  for the initial value  $\beta_j$  is the same for both parameterizations, we transform the Gaussian prior for  $\sqrt{\theta_j}|\xi_j^2$  to the corresponding gamma prior for  $\theta_j|\xi_j^2$  in the centered parameterization, see (11). In Step (c-2), the posteriors of  $\theta_j$  and  $\beta_j$  in the centered parameterization, conditional on the state process  $\beta_{j0}, \dots, \beta_{jT}$ , are easily obtained. First, the conditional posterior

$$p(\theta_j|\beta_{j0}, \dots, \beta_{jT}, \beta_j, \xi_j^2, P_{0,jj}) \propto p(\theta_j|\xi_j^2)p(\beta_{j0}|\beta_j, \theta_j, P_{0,jj}) \prod_{t=1}^T p(\beta_{jt}|\beta_{j,t-1}, \theta_j),$$

where  $\beta_{j0}|\beta_j, \theta_j, P_{0,jj} \sim \mathcal{N}(\beta_j, \theta_j P_{0,jj})$  and  $\beta_{jt}|\beta_{j,t-1}, \theta_j \sim \mathcal{N}(\beta_{j,t-1}, \theta_j)$ , is the density of a generalized inverse Gaussian distribution (GIG) with following parameters:

$$\theta_j|\beta_{j0}, \dots, \beta_{jT}, \beta_j, \xi_j^2, P_{0,jj} \sim \mathcal{GIG}\left(-\frac{T}{2}, \frac{1}{\xi_j^2}, \sum_{t=1}^T (\beta_{jt} - \beta_{j,t-1})^2 + \frac{(\beta_{j0} - \beta_j)^2}{P_{0,jj}}\right). \quad (18)$$

Note that sampling the process variance  $\theta_j$  from this GIG posterior<sup>6</sup> deviates from the usual MCMC inference for the centered state space model, since the conditionally conjugate inverted gamma prior (10) is substituted by a prior from the gamma distribution. Second, the posterior  $p(\beta_j|\beta_{j0}, \theta_j, \tau_j^2, P_{0,jj})$  is a Gaussian distribution, obtained by combining the prior  $\beta_j|\tau_j^2 \sim \mathcal{N}(0, \tau_j^2)$  with the conditional likelihood  $\beta_{j0}|\beta_j, \theta_j, P_{0,jj} \sim \mathcal{N}(\beta_j, \theta_j P_{0,jj})$ :

$$\beta_j|\beta_{j0}, \theta_j, \tau_j^2, P_{0,jj} \propto \mathcal{N}\left(\frac{\beta_{j0}\tau_j^2}{\tau_j^2 + \theta_j P_{0,jj}}, \frac{\tau_j^2\theta_j P_{0,jj}}{\tau_j^2 + \theta_j P_{0,jj}}\right). \quad (19)$$

Sampling the parameters  $a^\tau$  and  $a^\xi$  in Step (d) is performed without conditioning on  $\tau_1, \dots, \tau_d$  and  $\xi_1, \dots, \xi_d$ . The acceptance probability for  $a^{\xi, \text{new}}$  reads:

$$\min \left\{ 1, \frac{p(a^{\xi, \text{new}})a^{\xi, \text{new}}}{p(a^\xi)a^\xi} \prod_{j=1}^d \frac{p(\sqrt{\theta_j}|a^{\xi, \text{new}}, \kappa^2)}{p(\sqrt{\theta_j}|a^\xi, \kappa^2)} \right\},$$

based on the marginal prior (14). A similar acceptance probability holds for  $a^{\tau, \text{new}}$ .

Sampling the latent prior variances  $\tau_j^2$  and  $\xi_j^2$  of the hierarchical shrinkage priors (17) and

---

<sup>6</sup>To sample from the GIG distribution, we use a method proposed by Hörmann and Leydold (2014) which is implemented in the R-package **GIGrvg** (Hörmann and Leydold, 2015). This method is especially reliable for TVP models where the scale parameters of the GIG distribution can be extremely small due to shrinkage and other samplers tend to fail.

(12) for  $\beta_j$  and  $\sqrt{\theta_j}$  in Step (e) is less standard and we briefly discuss sampling  $\xi_j^2$  (full details are given in Appendix A.1.1.3). The conditionally normal prior  $\sqrt{\theta_j}|\xi_j^2$  in (12) leads to a likelihood for  $\xi_j^2$  which is the kernel of an inverted gamma density. In combination with the gamma prior for  $\xi_j^2|a^\xi, \kappa^2$ , this leads to a posterior distribution arising from a generalized inverse Gaussian (GIG) distribution:  $\xi_j^2|\theta_j, a^\xi, \kappa^2 \sim \mathcal{GIG}(a^\xi - 1/2, a^\xi \kappa^2, \theta_j)$ . Finally, Step (f) has to be modified for the SV model defined in (5). To sample  $(h_0, \dots, h_T)$  as well as  $\mu$ ,  $\phi$ , and  $\sigma_\eta^2$ , we rely on Kastner and Frühwirth-Schnatter (2014) who developed an interweaving strategy for boosting MCMC estimation of SV models.<sup>7</sup>

## 4 Comparing shrinkage priors through log predictive density scores

Log predictive density scores (LPDS) are an often used scoring rule to compare models; see, e.g., Gneiting and Raftery (2007). Geweke and Keane (2007) introduced LPDS for model comparison of econometric models, see also Geweke and Amisano (2010) for an excellent review of Bayesian predictive analysis. In the present paper, we use log predictive density scores as a means of evaluating and comparing different shrinkage priors.

As common in this framework, the first  $t_0$  time series observations  $\mathbf{y}^{\text{tr}} = (y_1, \dots, y_{t_0})$  are used as a “training sample”, while evaluation is performed for the remaining time series observations  $y_{t_0+1}, \dots, y_T$ , based on the log predictive density:

$$\text{LPDS} = \log p(y_{t_0+1}, \dots, y_T | \mathbf{y}^{\text{tr}}) = \sum_{t=t_0+1}^T \log p(y_t | \mathbf{y}^{t-1}) = \sum_{t=t_0+1}^T \text{LPDS}_t^*. \quad (20)$$

In (20),  $p(y_t | \mathbf{y}^{t-1})$  is the one-step ahead predictive density for time  $t$  given  $\mathbf{y}^{t-1} = (y_1, \dots, y_{t-1})$  which is evaluated at the observed value  $y_t$ . The (individual) log predictive density scores  $\text{LPDS}_t^* = \log p(y_t | \mathbf{y}^{t-1})$  provide a tool to analyze performance separately for each observation  $y_t$ , whereas LPDS is an aggregated measure of performance for the entire time series.

As shown by Frühwirth-Schnatter (1995) in the context of selecting time-varying and fixed components for a basic structural state space model, LPDS can be interpreted as a log marginal likelihood based on the training sample prior  $p(\boldsymbol{\vartheta} | \mathbf{y}^{\text{tr}})$ , since

$$p(y_{t_0+1}, \dots, y_T | \mathbf{y}^{\text{tr}}) = \int p(y_{t_0+1}, \dots, y_T | \mathbf{y}^{\text{tr}}, \boldsymbol{\vartheta}) p(\boldsymbol{\vartheta} | \mathbf{y}^{\text{tr}}) d\boldsymbol{\vartheta},$$

where  $\boldsymbol{\vartheta}$  summarises the unknown model parameters, e.g.  $\boldsymbol{\vartheta} = (\beta_1, \dots, \beta_d, \sqrt{\theta_1}, \dots, \sqrt{\theta_d}, \sigma^2)$

---

<sup>7</sup>This step is easily incorporated into Algorithm 1 using the R-package `stochvol` (Kastner, 2016).

for the homoscedastic state space model. This provides a sound and coherent foundation for using the log predictive density score for model – or, in our context, rather prior – comparison.

To approximate the one-step ahead predictive density  $p(y_t|\mathbf{y}^{t-1})$ , we use Gaussian sum approximations, which are derived from the MCMC draws  $(\boldsymbol{\vartheta}^{(m)}, m = 1, \dots, M)$  from the posterior distribution  $p(\boldsymbol{\vartheta}|\mathbf{y}^{t-1})$  given information up to  $\mathbf{y}^{t-1}$ , i.e:

$$\text{LPDS}_t^* = \log p(y_t|\mathbf{y}^{t-1}) = \log \int p(y_t|\mathbf{y}^{t-1}, \boldsymbol{\vartheta}) p(\boldsymbol{\vartheta}|\mathbf{y}^{t-1}) d\boldsymbol{\vartheta} \approx \log \left( \frac{1}{M} \sum_{m=1}^M p(y_t|\mathbf{y}^{t-1}, \boldsymbol{\vartheta}^{(m)}) \right), \quad (21)$$

where the one-step ahead predictive density  $p(y_t|\mathbf{y}^{t-1}, \boldsymbol{\vartheta})$  is Gaussian conditional on knowing  $\boldsymbol{\vartheta}$ .

We derive an approximation, called the *conditionally optimal Kalman mixture approximation*, which exploits the fact that the TVP model is a conditionally Gaussian state space model given  $\boldsymbol{\vartheta} = (\beta_1, \dots, \beta_d, \sqrt{\theta_1}, \dots, \sqrt{\theta_d}, \sigma_t^2)$ .<sup>8</sup> For each draw  $\boldsymbol{\vartheta}^{(m)} = (\beta_1^{(m)}, \dots, \beta_d^{(m)}, \sqrt{\theta_1^{(m)}}, \dots, \sqrt{\theta_d^{(m)}}, \sigma_t^{2(m)})$  from the posterior  $p(\boldsymbol{\vartheta}|\mathbf{y}^t)$ , we determine the *exact* predictive density  $p(y_t|\mathbf{y}^{t-1}, \boldsymbol{\vartheta}^{(m)})$  given by the normal distribution  $y_t|\mathbf{y}^{t-1}, \boldsymbol{\vartheta}^{(m)} \sim \mathcal{N}_d(\hat{y}_t^{(m)}, S_t^{(m)})$ , where  $\hat{y}_t^{(m)}$  and  $S_t^{(m)}$  are obtained from the prediction step of the Kalman filter (see Appendix A.1.2.1), based on the filtering density  $\tilde{\boldsymbol{\beta}}_{t-1}|\mathbf{y}^{t-1}, \boldsymbol{\vartheta}^{(m)} \sim \mathcal{N}_d(\mathbf{m}_{t-1}^{(m)}, \mathbf{C}_{t-1}^{(m)})$ :

$$\begin{aligned} \hat{y}_t^{(m)} &= \mathbf{x}_t \boldsymbol{\beta}^{(m)} + \mathbf{F}_t^{(m)} \mathbf{m}_{t-1}^{(m)}, \\ S_t^{(m)} &= \mathbf{F}_t^{(m)} (\mathbf{C}_{t-1}^{(m)} + \mathbf{I}_d) \mathbf{F}_t'^{(m)} + \sigma_t^{2(m)}, \end{aligned}$$

where  $\mathbf{F}_t^{(m)} = \mathbf{x}_t \text{Diag}(\sqrt{\theta_1^{(m)}}, \dots, \sqrt{\theta_d^{(m)}})$  and  $\mathbf{I}_d$  is the  $d \times d$  identity matrix. This yields the following Gaussian mixture approximation for  $p(y_t|\mathbf{y}^{t-1})$ :

$$p(y_t|\mathbf{y}^{t-1}) \approx \frac{1}{M} \sum_{m=1}^M f_N(y_t; \hat{y}_t^{(m)}, S_t^{(m)}). \quad (22)$$

Draws from  $p(\boldsymbol{\vartheta}|\mathbf{y}^{t-1})$  are obtained by running the Gibbs sampler outlined in Algorithm 1 for the reduced sample  $\mathbf{y}^{t-1} = (y_1, y_2, \dots, y_{t-1})$ . For a homoscedastic error specification,  $\sigma_t^{2(m)} \equiv \sigma^2$ , whereas  $\sigma_t^{2(m)}$  is forecasted in the following way for the SV model (5). Given the posterior draw  $h_{t-1}^{(m)}$ , we simulate  $h_t^{(m)}$  from a conditional normal distribution with mean  $\mu^{(m)} + \phi^{(m)}(h_{t-1}^{(m)} - \mu^{(m)})$  and variance  $\sigma_\eta^{2(m)}$  and define  $\sigma_t^{2(m)} = e^{h_t^{(m)}}$ .

---

<sup>8</sup>Alternative approximations are discussed in Appendix A.1.2.2.

## 5 Extension to multivariate time series

### 5.1 Sparse TVP models for multivariate time series

The methods introduced in the previous sections are easily extended to TVP models for multivariate time series, such as time-varying parameter VARs, see e.g. Eisenstat et al. (2014) who analyze the response of macro variables to fiscal shocks, and time-varying structural VARs, see e.g. Primiceri (2005) for a monetary policy application. Consider, as illustration, the following TVP model for an  $r$ -dimensional time series  $\mathbf{y}_t$ ,

$$\mathbf{y}_t = \mathbf{B}_t \mathbf{x}_t + \boldsymbol{\varepsilon}_t, \quad \boldsymbol{\varepsilon}_t \sim \mathcal{N}_r(\mathbf{0}, \boldsymbol{\Sigma}_t), \quad (23)$$

where  $\mathbf{x}_t$  is a *column* vector of  $d$  regressors, and  $\mathbf{B}_t$  is a time-varying  $(r \times d)$  matrix with coefficient  $\beta_{ij,t}$  in row  $i$  and column  $j$ , potentially containing structural zeros or constant values such that  $\beta_{ij,t} \equiv c$  apriori. The (apriori) unconstrained time-varying coefficients  $\beta_{ij,t}$  are assumed to follow independent random walks as in the univariate case:

$$\beta_{ij,t} = \beta_{ij,t-1} + \omega_{ij,t}, \quad \omega_{ij,t} \sim \mathcal{N}(0, \theta_{ij}), \quad (24)$$

with initial value  $\beta_{ij,0} \sim \mathcal{N}(\beta_{ij}, \theta_{ij} P_{0,ijj})$ , where  $P_{0,ijj} \sim \mathcal{G}^{-1}(\nu_P, (\nu_P - 1)c_P)$  as before. Both the fixed regression coefficients  $\beta_{ij}$  as well as the process variances  $\theta_{ij}$  are assumed to be unknown.

Each of the apriori unconstrained coefficients  $\beta_{ij,t}$  is potentially constant, with the corresponding process variance  $\theta_{ij}$  being 0. A constant coefficient  $\beta_{ij,t} \equiv \beta_{ij}$  is potentially insignificant, in which case  $\beta_{ij} = 0$ . Hence, shrinkage priors as introduced in Section 2.2 for the univariate case, are imposed on the  $\theta_{ij}$ s and  $\beta_{ij}$ s to define a sparse TVP model for identifying which of these scenarios holds for each coefficient  $\beta_{ij,t}$ .

For  $i = 1, \dots, r$ , the hierarchical double gamma prior for the process variances  $\theta_{ij}$  of the coefficients in the  $i$ th row of a multivariate TVP model reads:

$$\theta_{ij} | \xi_{ij}^2 \sim \mathcal{G}\left(\frac{1}{2}, \frac{1}{2\xi_{ij}^2}\right), \quad \xi_{ij}^2 | a_i^\xi, \kappa_i^2 \sim \mathcal{G}\left(a_i^\xi, a_i^\xi \kappa_i^2 / 2\right), \quad \kappa_i^2 \sim \mathcal{G}(d_1, d_2), \quad a_i^\xi \sim \mathcal{E}(b^\xi), \quad (25)$$

with prior expectation  $\xi_{ij}^2$  for each process variance  $\theta_{ij}$ . Similarly, an individual prior variance  $\tau_{ij}^2$  is introduced for each fixed regression coefficient  $\beta_{ij}$  as in (17):

$$\beta_{ij} | \tau_{ij}^2 \sim \mathcal{N}(0, \tau_{ij}^2), \quad \tau_{ij}^2 | a_i^\tau, \lambda_i^2 \sim \mathcal{G}(a_i^\tau, a_i^\tau \lambda_i^2 / 2), \quad \lambda_i^2 \sim \mathcal{G}(e_1, e_2), \quad a_i^\tau \sim \mathcal{E}(b^\tau). \quad (26)$$

By choosing  $a_i^\tau = a_i^\xi = 1$  in (25) and (26), a hierarchical Bayesian Lasso prior for multivariate TVP models results.



We assume row specific hyperparameters  $a_i^\tau, \lambda_i^2$  and  $a_i^\xi, \kappa_i^2$ , drawn from common hyperpriors with fixed hyperparameters  $e_1, e_2, b^\tau$  and  $d_1, d_2, b^\xi$ . This leads to prior independence across the  $r$  rows of the observation equation (23) and is advantageous for computational reasons, in particular, if the errors  $\boldsymbol{\varepsilon}_t$  are uncorrelated, i.e.  $\boldsymbol{\Sigma}_t$  is a diagonal matrix. In this case, the multivariate TVP model has a representation as  $r$  independent univariate TVP models as in Section 2.1 and MCMC estimation using Algorithm 1 can be performed independently for each of the  $r$  rows of the system, e.g. in a parallel computing environment.

If  $\boldsymbol{\Sigma}_t$  is a full covariance matrix, then the rows are not independent, because of the correlation among the various components in  $\boldsymbol{\varepsilon}_t$ . However, as shown by Lopes et al. (2016), a Cholesky decomposition of  $\boldsymbol{\Sigma}_t$  leads to such a representation, see also Eisenstat et al. (2014) and Zhao et al. (2016). Further details are provided in the next subsection.

## 5.2 The sparse TVP Cholesky SV model

Lopes et al. (2016) demonstrate how a multivariate time series  $\mathbf{y}_t \sim \mathcal{N}_r(\mathbf{0}, \boldsymbol{\Sigma}_t)$  with time-varying covariance matrix  $\boldsymbol{\Sigma}_t$  can be transformed into a system of  $r$  independent equations using the time-varying Cholesky decomposition  $\boldsymbol{\Sigma}_t = \mathbf{A}_t \mathbf{D}_t \mathbf{A}_t'$ , where  $\mathbf{A}_t \mathbf{D}_t^{1/2}$  is the lower triangular Cholesky decomposition of  $\boldsymbol{\Sigma}_t$ .  $\mathbf{A}_t$  is lower triangular with ones on the main diagonal, while  $\mathbf{D}_t$  is a time-varying diagonal matrix. It follows that  $\mathbf{A}_t^{-1} \mathbf{y}_t \sim \mathcal{N}_r(\mathbf{0}, \mathbf{D}_t)$ . Denoting the elements of  $\mathbf{A}_t^{-1}$  as  $\Phi_{ij,t}$ , for  $j < i$ , this can be expressed as

$$\begin{pmatrix} 1 & \dots & & & 0 \\ \Phi_{21,t} & 1 & & & 0 \\ & & \ddots & & 0 \\ \vdots & & & 1 & 0 \\ \Phi_{r1,t} & \Phi_{r2,t} & \dots & \Phi_{r,r-1,t} & 1 \end{pmatrix} \begin{pmatrix} y_{1t} \\ y_{2t} \\ \vdots \\ y_{rt} \end{pmatrix} \sim \mathcal{N}_r(\mathbf{0}, \mathbf{D}_t),$$

which can be written as in (23):

$$\mathbf{y}_t \sim \mathcal{N}_r(\mathbf{B}_t \mathbf{x}_t, \mathbf{D}_t), \quad (27)$$

where  $\mathbf{B}_t$  is a  $r \times (r-1)$  matrix with elements  $\beta_{ij,t} = -\Phi_{ij,t}$ ,  $\mathbf{D}_t$  is a diagonal matrix and the  $(r-1)$ -dimensional vector  $\mathbf{x}_t = (y_{1t}, \dots, y_{r-1,t})'$  is a regressor derived from  $\mathbf{y}_t$ . Thus the distribution of  $\mathbf{y}_t$  can be represented by a system of  $r$  independent TVP models as in Section 5.1, where each time-varying coefficient  $\beta_{ij,t}, j < i, i = 1, \dots, r$ , follows a random walk as in (24). Employing the prior (26) for  $\beta_{ij}$  and (25) for  $\theta_{ij}$  yields the sparse TVP

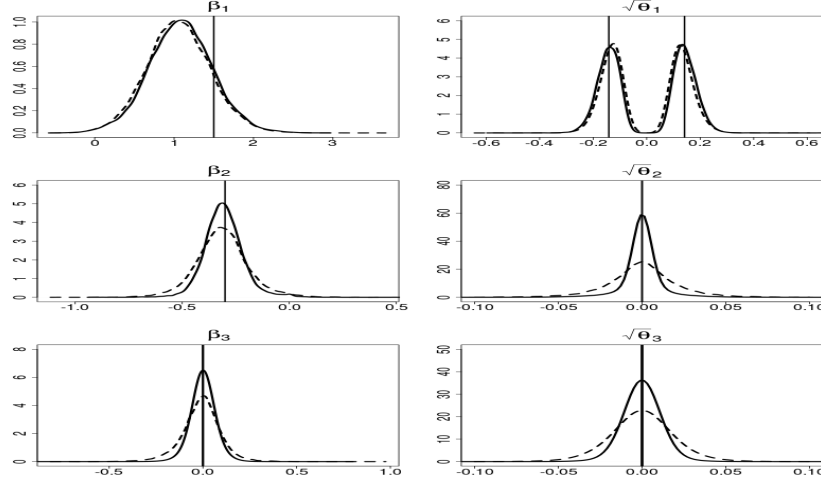


Figure 3: Simulated data. Posterior densities of  $\beta_j$  (left-hand side) and  $\sqrt{\theta_j}$  (right-hand side) together with the true values (indicated by the vertical lines), based on the hierarchical double gamma prior with  $a^\tau \sim \mathcal{E}(10)$  and  $a^\xi \sim \mathcal{E}(10)$  (solid line) and the hierarchical Bayesian Lasso prior (dashed line).

Cholesky SV model.

To capture conditional heteroscedasticity, the matrix  $\mathbf{D}_t = \text{Diag}(e^{h_{1t}}, \dots, e^{h_{rt}})$  is assumed to be time-varying, where for each row  $i = 1, \dots, r$ , the log volatility  $h_{it}$  is assumed to follow an individual SV model as in (5), with row specific parameters  $\mu_i$ ,  $\phi_i$ , and  $\sigma_{\eta,i}^2$ :

$$h_{it}|h_{i,t-1}, \mu_i, \phi_i, \sigma_{\eta,i}^2 \sim \mathcal{N}(\mu_i + \phi_i(h_{i,t-1} - \mu_i), \sigma_{\eta,i}^2).$$

For  $r = 3$ , for instance, the TVP Cholesky SV model reads:

$$\begin{aligned} y_{1t} &= \varepsilon_{1t}, & \varepsilon_{1t} &\sim \mathcal{N}(0, e^{h_{1t}}), \\ y_{2t} &= \beta_{21,t}y_{1t} + \varepsilon_{2t}, & \varepsilon_{2t} &\sim \mathcal{N}(0, e^{h_{2t}}), \\ y_{3t} &= \beta_{31,t}y_{1t} + \beta_{32,t}y_{2t} + \varepsilon_{3t}, & \varepsilon_{3t} &\sim \mathcal{N}(0, e^{h_{3t}}). \end{aligned}$$

No intercept is present in these TVP models. For the TVP model in the first row, no regressors are present and only the time-varying volatilities  $h_{1t}$  have to be estimated. In the  $i$ -th equation,  $i - 1$  regressors are present and  $d = i - 1$  time-varying regression coefficients  $\beta_{ij,t}$  as well as the time-varying volatilities  $h_{it}$  need to be estimated. Each of these equations is transformed into a non-centered TVP model and the MCMC scheme in Algorithm 1 is applied to perform Bayesian inference independently for each row  $i$ .

## 6 Illustrative Application to Simulated Data

To illustrate our methodology for simulated data, we generated 100 univariate time series of length  $T = 200$  from a TVP model where  $d = 3$ ,  $\{x_{1t}\} \equiv 1$ ,  $\{x_{jt}\} \sim \mathcal{N}(0, 1)$  for  $j = 2, 3$ ,  $\sigma^2 = 1$ ,  $(\beta_1, \beta_2, \beta_3) = (1.5, -0.3, 0)$  and  $(\theta_1, \theta_2, \theta_3) = (0.02, 0, 0)$ . For each time series,  $\beta_{1t}$  is a strongly time-varying coefficient,  $\beta_{2t}$  is a constant, but significant coefficient, and  $\beta_{3t}$  is an insignificant coefficient. As shrinkage priors on  $\beta_j$  and  $\sqrt{\theta_j}$ , we consider the hierarchical double gamma prior with  $a^\tau \sim \mathcal{E}(10)$  and  $a^\xi \sim \mathcal{E}(10)$  and the hierarchical Bayesian Lasso prior (that is  $a^\tau = a^\xi = 1$ ) under the hyperparameter setting  $d_1 = d_2 = e_1 = e_2 = 0.001$ . For each of the 100 simulated time series, MCMC estimation is based on Algorithm 1 by drawing  $M = 30,000$  samples after a burn-in of length 30,000.<sup>9</sup> In Figure 3 we compare the posterior densities for  $\beta_j$  and  $\sqrt{\theta_j}$  for one such time series under both shrinkage priors. In general, we want to distinguish three types of coefficients: time-varying, static but significant, and insignificant. One way to achieve a classification is by visual inspection of the posterior distributions of  $\beta_j$  and  $\sqrt{\theta_j}$ . The posterior density of the scale parameter  $\sqrt{\theta_j}$  is symmetric around zero by definition. Thus, if the unknown variance  $\theta_j$  is different from zero, then the posterior density of  $\sqrt{\theta_j}$  is likely to be bimodal. If we find that the posterior density of  $\sqrt{\theta_j}$  is unimodal, then the unknown variance is likely to be zero.

While such a bimodal structure of  $p(\sqrt{\theta_j}|\mathbf{y})$  is well pronounced for the first coefficient where  $\sqrt{\theta_1} = 0.141$ ,  $p(\sqrt{\theta_j}|\mathbf{y})$  is indeed shrunk toward zero for the two coefficients with zero variances  $\theta_2 = \theta_3 = 0$ . For the third coefficient, where in addition  $\beta_3 = 0$ , also the posterior  $p(\beta_3|\mathbf{y})$  is shrunk toward zero. Further, we show the posterior paths of  $\beta_{jt}$  in Figure 4. Evidently, shrinkage priors are able to detect the time-varying coefficient  $\beta_{1t}$ , the constant but significant coefficient  $\beta_{2t}$  and the insignificant coefficient  $\beta_{3t}$ . In both figures, the advantage of the double gamma prior compared to the Bayesian Lasso prior is reflected by increased efficiency in identifying coefficients that are not time-varying.

Table 1 summarises the average mean squared error ( $avMSE$ ), the average squared bias ( $avBIAS^2$ ) and the average variance ( $avVAR$ ) for the parameters  $\beta_1, \beta_2, \beta_3, |\sqrt{\theta_1}|, |\sqrt{\theta_2}|$ , and  $|\sqrt{\theta_3}|$  over the 100 simulated time series.<sup>10</sup> Heavier shrinkage introduced by the hierarchical double gamma prior leads to reduced  $avMSE$  compared to the hierarchical Bayesian Lasso prior, in particular for the two coefficients which are not time-varying.

<sup>9</sup>The Bayesian Lasso prior is combined with the ASIS strategy by fixing  $a^\tau = a^\xi = 1$  and skipping Step (d).

<sup>10</sup>Given  $M$  draws  $\vartheta^{(i1)}, \dots, \vartheta^{(iM)}$ , of a parameter  $\vartheta$  for each time series  $i$ , these measures are defined as  $avMSE = avVAR + avBIAS^2$ , where  $avVAR = \frac{1}{100} \sum_{i=1}^{100} V_i$  and  $avBIAS^2 = \frac{1}{100} \sum_{i=1}^{100} (E_i - \vartheta^{\text{true}})^2$  with  $E_i = \frac{1}{M} \sum_{m=1}^M \vartheta^{(im)}$  and  $V_i = \frac{1}{M} \sum_{m=1}^M (\vartheta^{(im)} - E_i)^2$ .

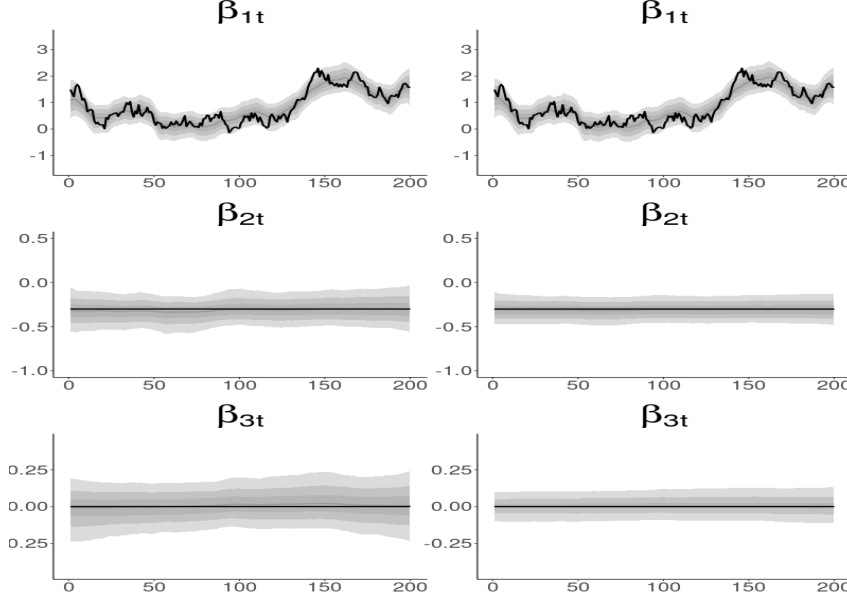


Figure 4: Simulated data. Pointwise (0.025, 0.25, 0.5, 0.75, 0.975)-quantiles of the posterior paths  $\beta_{jt} = \beta_j + \sqrt{\theta_j} \tilde{\beta}_{jt}$  in the centered parametrization in comparison to the true paths (thick black line) for one of the simulated time series; left-hand side: hierarchical Bayesian Lasso prior, right-hand side: hierarchical double gamma prior with  $a^\tau \sim \mathcal{E}(10)$  and  $a^\xi \sim \mathcal{E}(10)$ .

	$a^\tau \sim \mathcal{E}(10), a^\xi \sim \mathcal{E}(10)$			$a^\tau = a^\xi = 1$		
	$avMSE$	$avVAR$	$avBIAS^2$	$avMSE$	$avVAR$	$avBIAS^2$
$\beta_1$	3.30E-01	1.67E-01	1.63E-01	3.60E-01	1.57E-01	2.03E-01
$\beta_2$	8.18E-03	8.11E-03	6.47E-05	1.56E-02	1.55E-02	1.77E-04
$\beta_3$	2.10E-03	2.10E-03	1.36E-06	1.14E-02	1.13E-02	1.31E-04
$ \sqrt{\theta_1} $	1.81E-03	1.79E-03	2.50E-05	1.61E-03	1.56E-03	5.32E-05
$ \sqrt{\theta_2} $	1.14E-04	9.33E-05	2.11E-05	5.02E-04	2.47E-04	2.55E-04
$ \sqrt{\theta_3} $	4.33E-05	3.53E-05	7.97E-06	3.10E-04	1.44E-04	1.66E-04

Table 1: Simulated data. Average mean squared error ( $avMSE$ ), average variance ( $avVAR$ ), and average squared bias ( $avBIAS^2$ ) over 100 simulated time series for the hierarchical double gamma prior with  $a^\tau \sim \mathcal{E}(10)$  and  $a^\xi \sim \mathcal{E}(10)$  and the hierarchical Bayesian Lasso prior with  $a^\tau = a^\xi = 1$ .

## 7 Applications in Economics and Finance

### 7.1 Modelling EU area inflation

As a first application, we reconsider EU-area inflation data analyzed in Belmonte et al. (2014) and consider the generalized Phillips curve specification, where inflation  $\pi_t$  depends

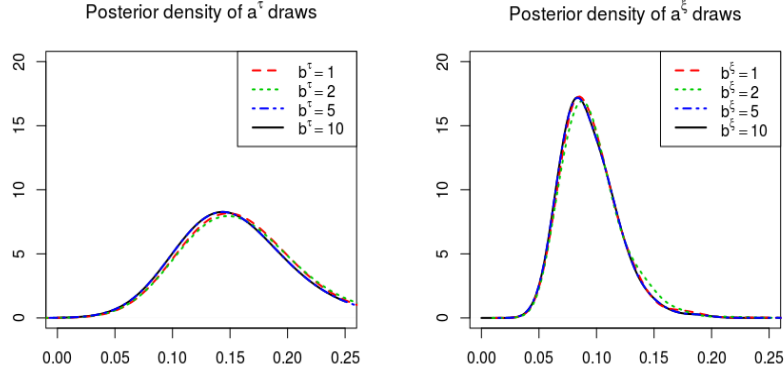


Figure 5: ECB data. Posterior density of  $a^\tau$  (left-hand side) and  $a^\xi$  (right-hand side).

on (typically  $p = 12$ ) lags of inflation and other predictors  $\mathbf{z}_t$ :

$$\pi_{t+h} = \sum_{j=0}^{p-1} \phi_{jt} \pi_{t-j} + \mathbf{z}_t \boldsymbol{\gamma}_t + \varepsilon_{t+h}, \quad \varepsilon_{t+h} \sim \mathcal{N}(0, \sigma^2). \quad (28)$$

This set-up has been discussed by Stock and Watson (2012), among others, for forecasting the annual inflation rate, that is  $h = 12$ . Data are monthly and range from February 1994 until November 2010, i.e.  $T = 190$ . We list precise definitions of all variables in Appendix A.2.1. As the time series are not seasonally adjusted, we include monthly dummy variables as covariates in (28) to account for seasonal patterns. Thus we are estimating in total  $d = 37$  possibly time-varying coefficients, consisting of the intercept, 13 regressors like the *unemployment rate* and the *1-month interest rate*, 12 lagged values of inflation and 11 seasonal dummies.

As shrinkage priors on  $\beta_j$  and  $\sqrt{\theta_j}$ , we consider the hierarchical double gamma prior with  $a^\tau \sim \mathcal{E}(b^\tau)$  and  $a^\xi \sim \mathcal{E}(b^\xi)$  under the hyperparameter setting  $d_1 = d_2 = e_1 = e_2 = 0.001$  and compare it with the hierarchical Bayesian Lasso prior (that is  $a^\tau = a^\xi = 1$ ) applied by Belmonte et al. (2014). For each prior, MCMC inference is based on Algorithm 1 with  $M = 100,000$  draws after a burn-in of the same size. For the hierarchical double gamma prior, we considered various hyperparameters  $b^\tau$  and  $b^\xi$  and the corresponding posterior densities of  $a^\tau$  and  $a^\xi$  are shown in Figure 5, with posterior summaries being provided in Table 2. The acceptance probability for the random walk MH algorithm in Step (d) of Algorithm 1 lies in the range of 0.24 to 0.26. For these data, the posteriors of  $a^\tau$  and  $a^\xi$  clearly point at the double gamma prior rather than the Bayesian Lasso prior. The choice of the hyperparameters  $b^\tau$  and  $b^\xi$  does not play a significant role and the following results are presented for  $b^\tau = b^\xi = 10$ .

$b^\tau = b^\xi$	$p(a^\tau \mathbf{y})$				$p(a^\xi \mathbf{y})$			
	1st Qu.	Median	Mean	3rd Qu.	1st Qu.	Median	Mean	3rd Qu.
1	0.128	0.153	0.158	0.181	0.078	0.091	0.094	0.107
2	0.127	0.151	0.158	0.181	0.078	0.092	0.096	0.109
5	0.124	0.147	0.153	0.174	0.076	0.090	0.094	0.107
10	0.122	0.145	0.150	0.172	0.074	0.088	0.090	0.103

Table 2: ECB data. Posterior summaries for  $p(a^\tau|\mathbf{y})$  and  $p(a^\xi|\mathbf{y})$  for various values  $b^\tau = b^\xi$ .

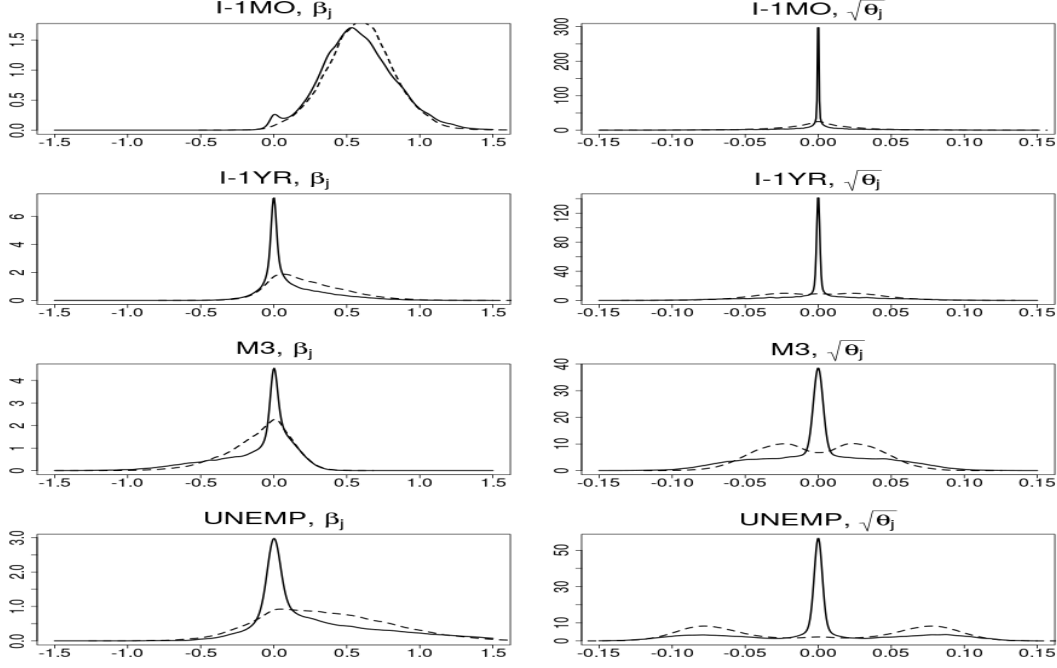


Figure 6: ECB data. Posterior densities of  $\beta_j$  (left-hand side) and  $\sqrt{\theta_j}$  (right-hand side), based on the hierarchical double gamma prior with  $a^\tau \sim \mathcal{E}(10)$  and  $a^\xi \sim \mathcal{E}(10)$  (solid line) and the hierarchical Bayesian Lasso prior (dashed line) for following predictors (from top to bottom): *1-month interest rate*, *1-year interest rate*, *M3*, and *unemployment rate*.

Summary statistics of  $p(\beta_j|\mathbf{y})$  and  $p(\sqrt{\theta_j}|\mathbf{y})$  for the hierarchical double gamma prior with  $a^\tau \sim \mathcal{E}(10)$  and  $a^\xi \sim \mathcal{E}(10)$  are given in Table A.3 in Appendix A.3.1. The easiest combination to spot is the case where both parameters  $\beta_j$  and  $\sqrt{\theta_j}$  are shrunk toward zero and the corresponding posterior densities exhibit peaks at zero. This is the case for most of the 37 covariates. The posterior median of  $\sqrt{|\theta_j|}$  in Table A.3 is smaller than  $10^{-3}$  for 34 regression coefficients, among them the lagged values of inflation and the monthly dummy variables. In addition, for these coefficients the 95%-confidence regions for  $\beta_j$  obtained from  $p(\beta_j|\mathbf{y})$  are reported in Table A.3 and show that none of these variables is “significant”.

The four variables in Table A.3 with a posterior mean of  $\sqrt{|\theta_j|}$  larger than  $10^{-2}$  are the

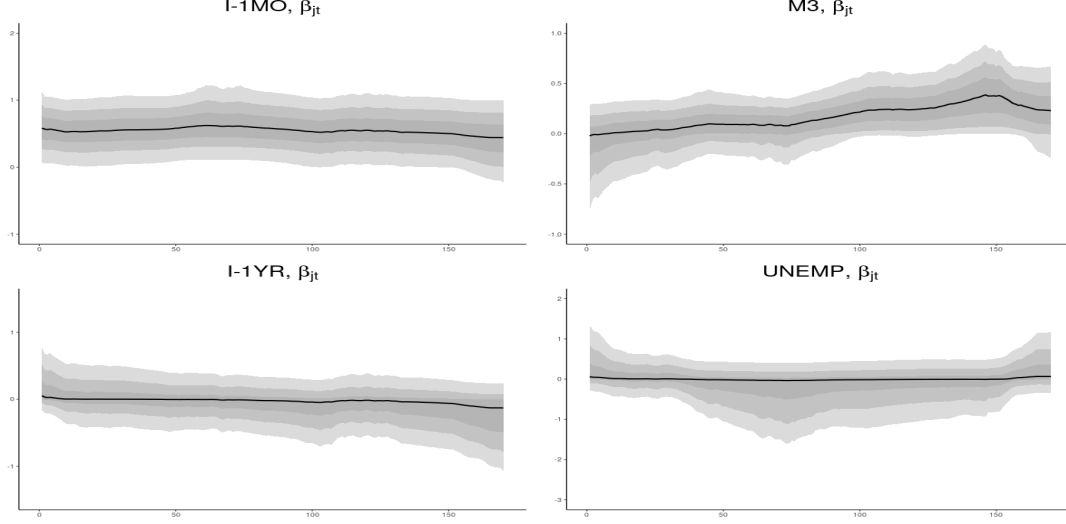


Figure 7: ECB data. Pointwise (0.025, 0.25, 0.5, 0.75, 0.975)-quantiles of the posterior paths of  $\beta_{jt} = \beta_j + \sqrt{\theta_j} \tilde{\beta}_{jt}$ , based on the hierarchical double gamma prior with  $a^\tau \sim \mathcal{E}(10)$  and  $a^\xi \sim \mathcal{E}(10)$ ; left-hand side: *1-month interest rate* (top) and *1-year interest rate* (bottom); right-hand side: *M3* (top) and *unemployment rate* (bottom).

*1-month interest rate* ( $j = 14$ ), the *1-year interest rate* ( $j = 15$ ), *M3* ( $j = 22$ ), and the *unemployment rate* ( $j = 26$ ). For illustration, we present the corresponding posterior densities of  $\beta_j$  and  $\sqrt{\theta_j}$  in Figure 6 under the hierarchical double gamma prior with  $a^\tau \sim \mathcal{E}(10)$  and  $a^\xi \sim \mathcal{E}(10)$  and the hierarchical Bayesian Lasso prior with  $a^\tau = a^\xi = 1$ . The corresponding posterior paths  $\beta_{jt} = \beta_j + \sqrt{\theta_j} \tilde{\beta}_{jt}$  are reported in Figure 7 for the hierarchical double gamma prior. A time-varying behaviour is visible for *M3* and the *unemployment rate*. The path of the *1-month interest rate* is significantly different from zero, but the posterior density of  $\sqrt{\theta_j}$  exhibits a peak at zero and indicates a constant coefficient. The *1-year interest rate* is basically shrunk toward zero and can be regarded as insignificant.

For this data set, full conditional MCMC sampling turned out to be extremely inefficient and motivated us to include the interweaving step in the Gibbs sampler outlined in Algorithm 1. For illustration, Figure 8 shows MCMC paths obtained for  $\beta_1$  with and without interweaving. As illustrated for selected parameters in Table 3, adding the interweaving step leads to substantial improvement of the mixing behaviour of MCMC sampling, with considerably reduced inefficiency factors.<sup>11</sup>

Finally, as discussed in Section 4, we use log predictive density scores (LPDS) to evaluate the various shrinkage priors. Figure 9 shows cumulative LPDS over the last 100 time points, using the conditionally optimal Kalman mixture approximation derived in

<sup>11</sup>Inefficiency factors were computed using the function `effectiveSize` from the R package `coda` (Plummer et al., 2006).

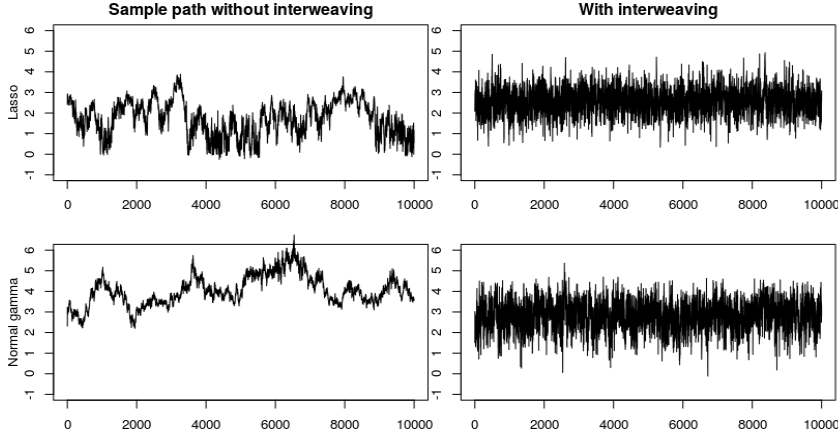


Figure 8: ECB data. Sample paths of  $\beta_1$  comparing the MCMC schemes without interweaving (left-hand side) and with interweaving (right-hand side) for  $a^\tau = a^\xi = 1$  (top row) and  $a^\tau \sim \mathcal{E}(10), a^\xi \sim \mathcal{E}(10)$  (bottom row).  $M = 100,000$  draws, only every tenth draw is shown.

$a^\tau \sim \mathcal{E}(10), a^\xi \sim \mathcal{E}(10)$					$a^\tau = a^\xi = 1$			
no ASIS		ASIS			no ASIS		ASIS	
$j$	$\beta_j$	$ \sqrt{\theta_j} $	$\beta_j$	$ \sqrt{\theta_j} $	$\beta_j$	$ \sqrt{\theta_j} $	$\beta_j$	$ \sqrt{\theta_j} $
1	4368	271	86	105	1464	185	72	71
14	535	367	77	231	53	57	28	57
15	116	280	109	245	143	197	45	76
22	1192	328	110	136	64	95	45	56
26	450	672	231	441	266	203	79	100

Table 3: ECB data. Inefficiency factors of MCMC posterior draws of selected parameters, obtained from Algorithm 1 with and without interweaving under the hierarchical double gamma prior with  $a^\tau \sim \mathcal{E}(10)$  and  $a^\xi \sim \mathcal{E}(10)$  and the hierarchical Bayesian Lasso prior.

Section 4.<sup>12</sup> Evidently, for this time series, the hierarchical double gamma prior is clearly preferable to the hierarchical Bayesian Lasso prior applied by Belmonte et al. (2014).

## 7.2 Sparse TVP Cholesky SV modelling of DAX returns

As a second real world data application, we fit the sparse TVP Cholesky SV model introduced in Section 5.2 to 29 indices from the German Stock Index DAX, see Appendix A.2.2 for more details on the data. The ordering of the indices is alphabetical and our data set spans roughly 2500 daily stock returns from September 4th, 2001 until August 31st,

<sup>12</sup>For numerical reasons, it is essential to use the conditionally optimal Kalman mixture approximation rather than the naive approximation to approximate the predictive density, see Appendix A.3.2 for details.



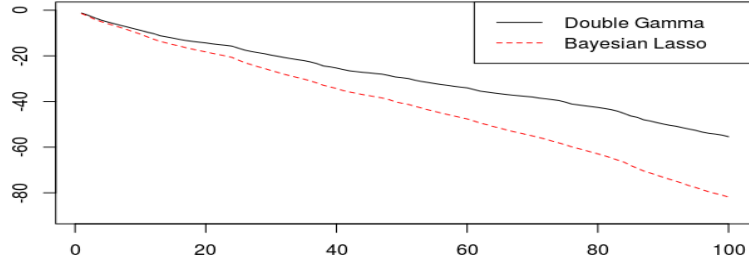


Figure 9: ECB data. Cumulative log predictive scores for the last 100 time point (labelled with time index  $t - t_0$ , where  $t_0 = 90$ ) under the hierarchical double gamma prior with  $a^\tau \sim \mathcal{E}(10)$  and  $a^\xi \sim \mathcal{E}(10)$  (solid line) and the hierarchical Bayesian Lasso prior (dashed line).

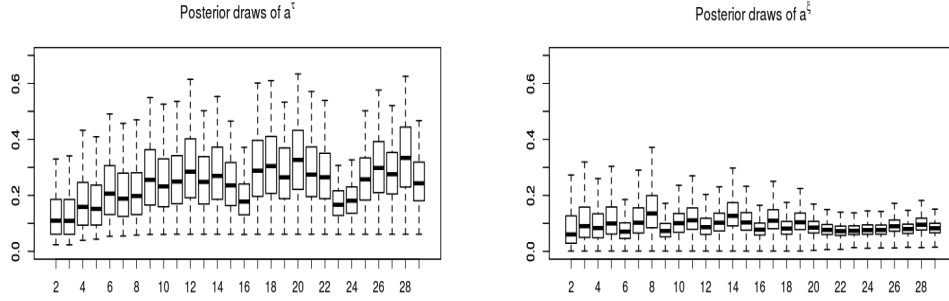


Figure 10: DAX data. Posterior densities of  $a_i^\tau$  (left-hand side) and  $a_i^\xi$  (right-hand side) under a hierarchical double gamma prior with  $a_i^\tau \sim \mathcal{E}(10)$  and  $a_i^\xi \sim \mathcal{E}(10)$ , represented by box plots for  $i = 2, \dots, 29$ . Whiskers correspond to the 0.05 and the 0.95 quantile.

2011.<sup>13</sup>

Due to the nature of the TVP Cholesky SV model, a representation of the multivariate model in terms of 29 independent equations exists. Exploiting representation (27), we estimate a pure stochastic volatility model for the first index and 28 TVP models with SV error specification for the remaining indices, with the dimension  $d$  increasing from 1 to 28. To estimate the resulting 406 potentially time-varying coefficients  $\beta_{ij,t}$  in an efficient manner, we apply the hierarchical double gamma priors introduced in (25) and (26) with  $a_i^\tau \sim \mathcal{E}(10)$  and  $a_i^\xi \sim \mathcal{E}(10)$  as well as the hierarchical Bayesian Lasso prior (that is  $a_i^\tau = a_i^\xi = 1$ ) under the hyperparameter setting  $d_1 = d_2 = e_1 = e_2 = 0.001$ . In

<sup>13</sup>As any model based on a Cholesky decomposition, inference is not invariant with respect to reordering the indices. While inference for the elements of  $\Sigma_t$  was fairly robust, we observed sensitivity to the ordering of the data for functionals of  $\Sigma_t^{-1}$ , e.g. the time-varying global minimum variance portfolio weights derived from  $\Sigma_t^{-1}$ .

addition to these shrinkage priors, we apply the usual conditionally conjugate prior, i.e.  $\theta_{ij} \sim \mathcal{IG}(s_0, S_0)$  for all process variances  $\theta_{ij}$  and  $\beta_{ij} \sim \mathcal{N}(0, A_0)$  for all fixed regression coefficients  $\beta_{ij}$ , with prior setting as in Petris et al. (2009), namely  $s_0 = 0.1$ ,  $S_0 = 0.001$  and  $A_0 = 10$ .

For all TVP models and all priors, MCMC inference is performed using Algorithm 1 with  $M = 50,000$  draws after a burn-in of 50,000.<sup>14</sup> The acceptance probability for the MH algorithm in Step (d) lies in the range of 0.24 to 0.26. Posterior densities of  $a_i^\tau$  and  $a_i^\xi$  under the hierarchical double gamma prior are provided in Figure 10. The posterior medians of  $a_i^\tau$  are in the range of 0.11 to 0.37, whereas the posterior medians of  $a_i^\xi$  lie between 0.07 and 0.15.

Exemplarily, detailed results are presented for the tenth time-varying regression in Figure 11, where we compare the posterior densities of  $\beta_{ij}$  and  $\sqrt{\theta_{ij}}$ , for  $i = 10$  and  $j = 1, \dots, 9$ , obtained under the different priors. As expected, under the inverted gamma prior all posteriors distributions of  $\sqrt{\theta_{ij}}$  are bounded away from 0, with the position of the symmetric posterior modes (roughly  $\pm 0.015$ ) being more or less the same for all coefficients.<sup>15</sup> As opposed to this, both shrinkage priors allow the posterior distribution of  $\sqrt{\theta_{ij}}$  to concentrate at 0, if appropriate, and in this way allows to distinguish between coefficients that are time-varying ( $j = 1, 2, 7$ ) and the remaining coefficients which turn out to be static. When comparing both shrinkage priors, the influence of the increased shrinkage introduced by the double gamma prior is evident for static coefficients, with the posterior of  $\sqrt{\theta_{ij}}$  showing a much more pronounced spike at 0 than the Bayesian Lasso prior.

For the static coefficients, the posterior distributions of  $\beta_{ij}$  indicate that some coefficients are significant, in particular when  $j = 3$  and  $j = 9$ , whereas others are clearly insignificant, e.g. when  $j = 6$ . These findings are confirmed by the corresponding posterior paths of  $\beta_{ij,t} = \beta_{ij} + \sqrt{\theta_{ij}}\tilde{\beta}_{ij,t}$  displayed in Figure 12 under the hierarchical double gamma prior and the inverted gamma prior. For the double gamma prior, the coefficients  $\beta_{i1,t}$ ,  $\beta_{i2,t}$ , and  $\beta_{i7,t}$  are the only ones that are time-varying, whereas  $\beta_{i3,t}$  and  $\beta_{i9,t}$  are constant, but shifted away from 0. Figure 12 also demonstrates a dramatic gain in statistical efficiency, in terms of dispersion of the posterior distribution of  $\beta_{ij,t}$  for each point in time, compared to the inverted gamma prior. This holds in particular for coefficients which are static, but significant such as  $\beta_{i3,t}$  and  $\beta_{i9,t}$ . In addition, the estimated paths are much smoother

<sup>14</sup>MCMC estimation under the inverted gamma prior requires a minor modification of Algorithm 1. We sample  $\theta_{ij}$  only in the centered parameterization from the conditional posterior  $\theta_{ij}|\beta \sim \mathcal{IG}\left(s_0 + \frac{T+1}{2}, S_0 + \frac{1}{2} \sum_{t=1}^T (\beta_{ij,t} - \beta_{ij,t-1})^2 + \frac{(\beta_{ij,0} - \beta_{ij})^2}{2P_{0,ijj}}\right)$ .

<sup>15</sup>The location of the posterior distribution is mainly driven by the prior – for the alternative hyperparameters  $s_0 = 0.5$  and  $S_0 = 0.2275$  (not shown in the figure) the posterior modes shift to around  $\pm 0.1$ .

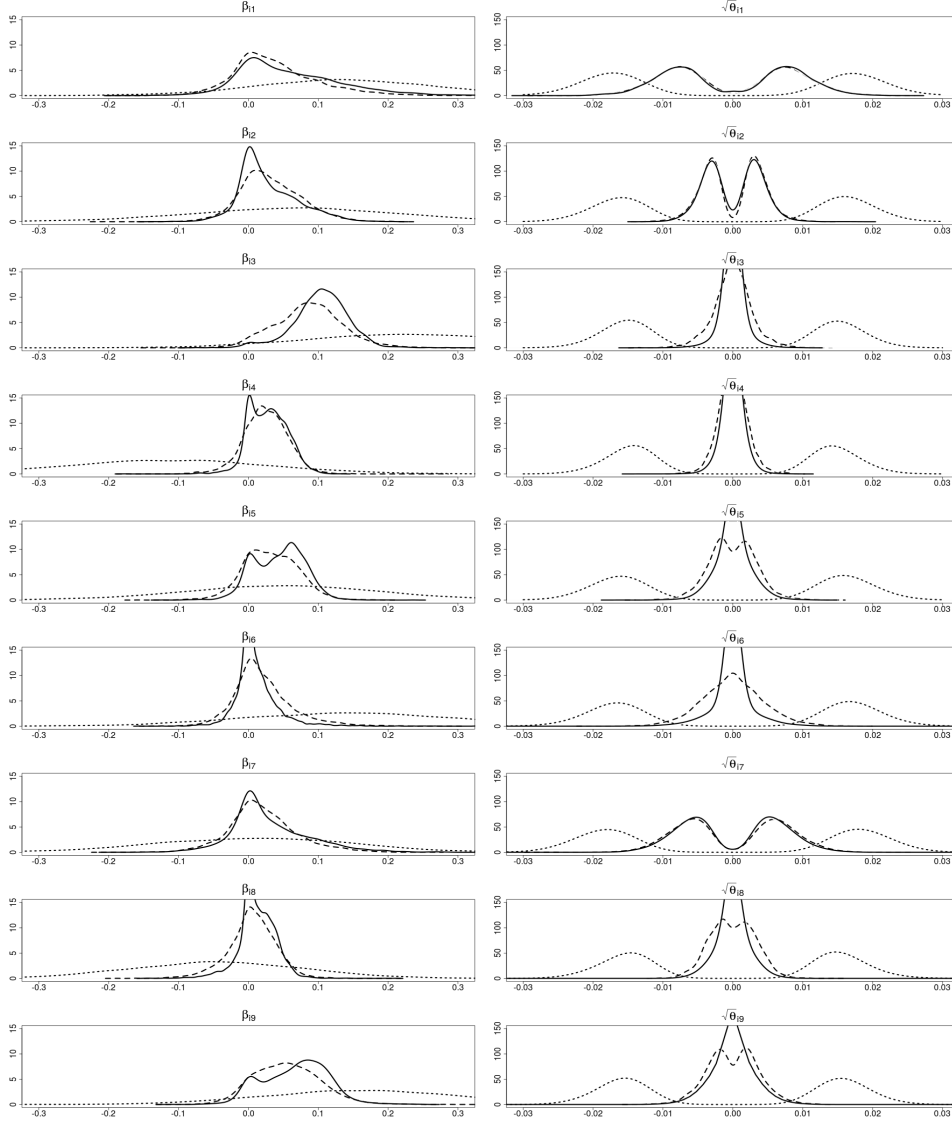


Figure 11: DAX data. Posterior densities of  $\beta_{ij}$  (left-hand side) and  $\sqrt{\theta_{ij}}$  (right-hand side) for  $i = 10$  and  $j = 1, \dots, 9$  (from top to bottom), derived under the conditionally conjugate prior  $\beta_{ij} \sim \mathcal{N}(0, 10)$  and  $\theta_{ij} \sim \mathcal{IG}(0.1, 0.001)$  (dotted line), the hierarchical Bayesian Lasso prior with  $a_i^\tau = a_i^\xi = 1$  (dashed line) and a hierarchical double gamma prior with  $a_i^\tau \sim \mathcal{E}(10)$  and  $a_i^\xi \sim \mathcal{E}(10)$  (solid line).

under the double gamma prior, which facilitates the interpretation of the time-varying components  $\beta_{i1,t}$ ,  $\beta_{i2,t}$ , and  $\beta_{i7,t}$ . The coefficient  $\beta_{i2,t}$ , for instance, shows a trending behaviour, which is not apparent under the inverted gamma prior.

Similar impact of our shrinkage method can be observed for the remaining 27 equations in the TVP model. Overall, we investigated all 406 posterior paths  $\beta_{ij,t}$ , together with the corresponding posterior distributions of  $\beta_{ij}$  and  $\sqrt{\theta_{ij}}$ , and found that a large fraction of these coefficients is not significant. For illustration, we display in Figure 13 one (out

of 2500) heat maps of the posterior median of the  $29 \times 28$  Cholesky factor matrix  $\mathbf{B}_t$  at  $t = 1150$ . Whereas the majority of the estimated coefficients  $\hat{\beta}_{ij,t}$  is different from zero for the inverted gamma prior, only a small part is significantly different from zero for the double gamma prior.

Finally, we compare the various priors using LPDS for the last 500 returns, with the first 400 observations serving as training sample. Very conveniently, the triangular structure of the model allows to decompose the 29-dimensional predictive density as  $p(\mathbf{y}_t|\mathbf{y}^{t-1}) = \prod_{i=1}^r p(y_{i,t}|\mathbf{y}^{t-1})$ . Hence, the overall log predictive density score  $\text{LPDS}_t^*$  at time  $t$  results as the sum of the individual log predictive density scores  $\text{LPDS}_{i,t}^* = \log p(y_{i,t}|\mathbf{y}^{t-1})$ , derived independently for each of the  $r = 29$  TVP models:

$$\text{LPDS}_t^* = \log p(\mathbf{y}_t|\mathbf{y}^{t-1}) = \sum_{i=1}^r \log p(y_{i,t}|\mathbf{y}^{t-1}) = \sum_{i=1}^r \text{LPDS}_{i,t}^*. \quad (29)$$

The individual log predictive density scores  $\text{LPDS}_{i,t}^*$  are approximated using the conditionally optimal Kalman mixture approximation introduced in Section 4 and the cumulative log predictive scores are shown in Figure 14 for the various priors. We find overwhelming evidence in favour of using shrinkage priors instead of the popular inverted gamma prior. For the later, the choice of the hyperparameters (see  $\theta_{ij} \sim \mathcal{IG}(0.1, 0.001)$  versus  $\theta_{ij} \sim \mathcal{IG}(0.5, 0.2275)$ ) exercises tremendous influence on the log predictive density scores. Figure 14 also compares the hierarchical Bayesian Lasso prior with the hierarchical double gamma prior with fixed values  $a^\tau = a^\xi = 0.1$ . Although the posteriors of  $a^\tau$  and  $a^\xi$  in Figure 10 clearly are bounded away from the values  $a^\tau = a^\xi = 1$  corresponding to the Bayesian Lasso prior, the log predictive density scores are very similar for both shrinkage priors.<sup>16</sup> Evidently, the major predictive gain comes from substituting the popular inverted gamma prior for the process variances by a sensible shrinkage prior that allows posterior concentration of the process variances at zero (see again Figure 11). As long as these priors behave sensibly at zero, the data contain little information to discriminate between them due to the small signal-to-noise ratio inherent in financial time series.

## 8 Conclusion

In the present paper, shrinkage for time-varying parameter (TVP) models was investigated within a Bayesian framework both for univariate and multivariate time series, with the aim to automatically reduce time-varying parameters to static ones, if the model is overfitting. This goal was achieved by formulating shrinkage priors for the process

---

<sup>16</sup>The posteriors in Figure 10 are based on the entire time series, but similar figures result for the last 500 observations.

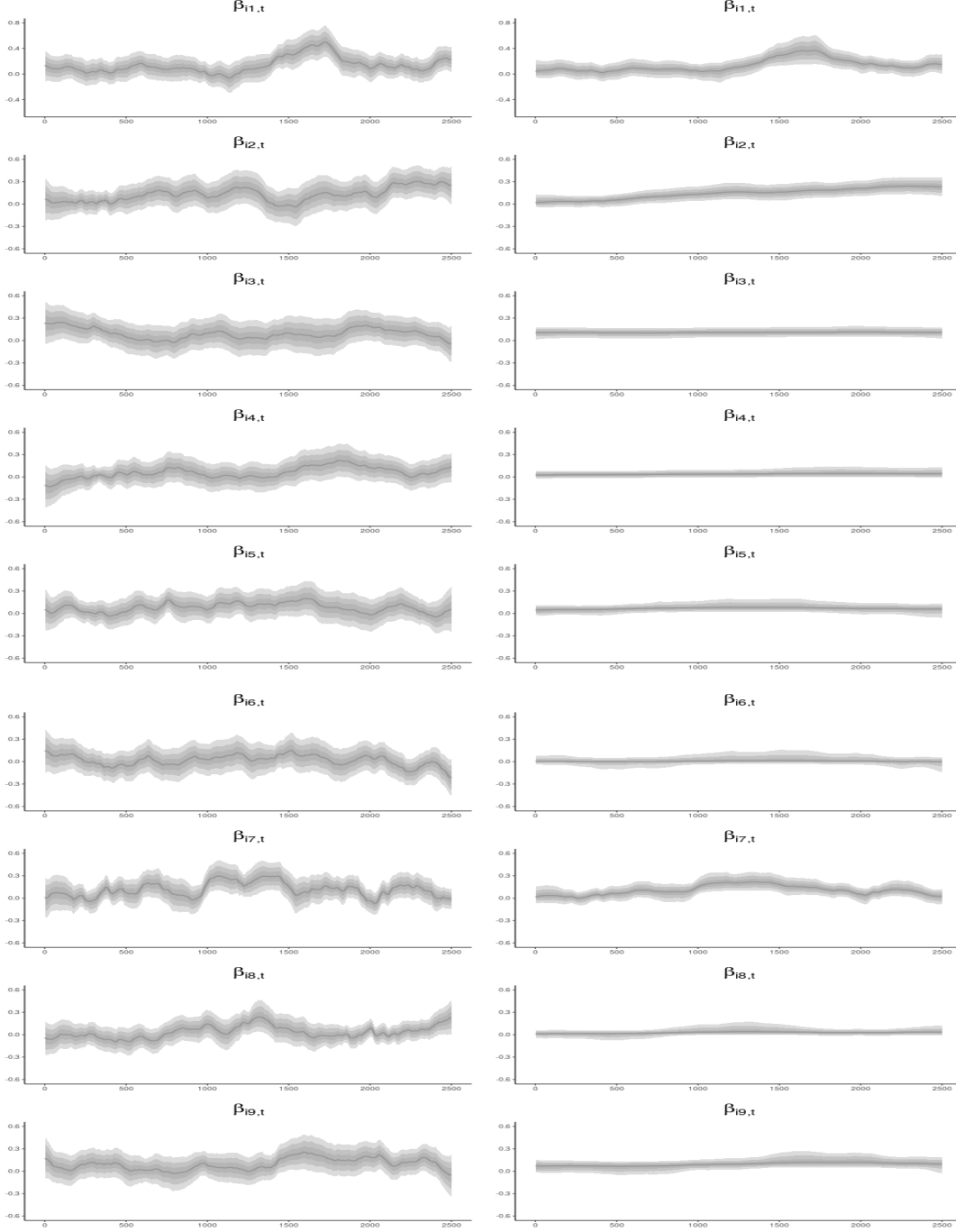


Figure 12: DAX data. Pointwise (0.025, 0.25, 0.5, 0.75, 0.975)-quantiles of the posterior paths  $\beta_{ij,t} = \beta_{ij} + \sqrt{\theta_{ij}}\tilde{\beta}_{ij,t}$  for  $i = 10$  and  $j = 1, \dots, 9$  (from top to bottom); derived under the conditionally conjugate prior  $\beta_{ij} \sim \mathcal{N}(0, 10)$  and  $\theta_{ij} \sim \mathcal{IG}(0.1, 0.001)$  (left-hand side) and a hierarchical double gamma prior with  $a^\tau \sim \mathcal{E}(10)$  and  $a^\xi \sim \mathcal{E}(10)$  (right-hand side).

variances based on the normal-gamma prior (Griffin and Brown, 2010), extending previous work using spike-and-slab priors (Frühwirth-Schnatter and Wagner, 2010) and the

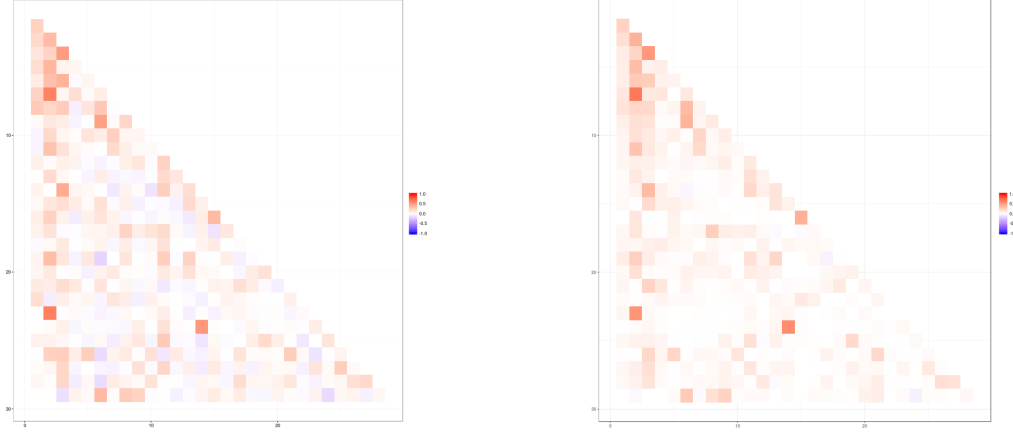


Figure 13: DAX data. Heat plot of the posterior median of the  $29 \times 28$  Cholesky factor matrix  $\mathbf{B}_t$  at  $t = 1150$ , derived under the conditionally conjugate prior  $\beta_{ij} \sim \mathcal{N}(0, 10)$  and  $\theta_{ij} \sim \mathcal{IG}(0.1, 0.001)$  (left-hand side) and a hierarchical double gamma prior with  $a^\tau \sim \mathcal{E}(10)$  and  $a^\xi \sim \mathcal{E}(10)$  (right-hand side). Values shrunk to zero are white.

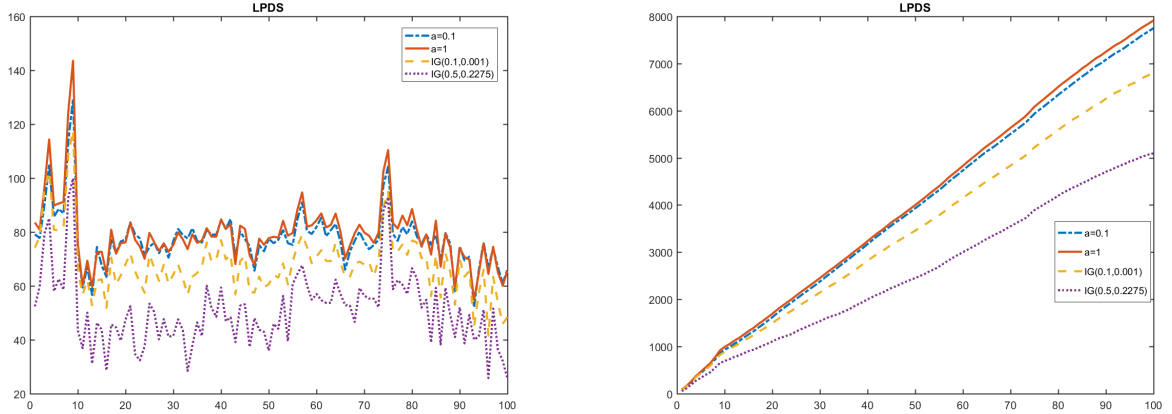


Figure 14: DAX data. Individual (left-hand side) and cumulative (right-hand side) log predictive density scores for the last 100 time points using the last 400 observations as training sample. Shrinkage prior with  $a^\tau = a^\xi = 1$  (full line) and  $a^\tau = a^\xi = 0.1$  (dash-dotted line) in comparison to the inverted gamma priors  $\theta_{ij} \sim \mathcal{IG}(0.1, 0.001)$  (dashed line) and  $\theta_{ij} \sim \mathcal{IG}(0.5, 0.2275)$  (dotted line).

Bayesian Lasso prior (Belmonte et al., 2014). As a major computational contribution, an efficient MCMC estimation scheme was developed, exploiting the ancillarity-sufficiency interweaving strategy of Yu and Meng (2011).

Our applications included EU area inflation modelling based on a TVP generalized Phillips curve and estimating a time-varying covariance matrix based on a sparse TVP Cholesky

SV model for a multivariate time series of returns of the DAX-30 index. We investigated different prior settings, including the popular inverted gamma prior for the process variances, using log predictive density scores. Overall, our findings suggest that the family of double gamma priors introduced in this paper for sparse TVP models is successful in avoiding overfitting, if coefficients are, indeed, static or even insignificant. The framework developed in this paper is very general and holds the promise to be useful for introducing sparsity in other TVP and state space models in many different settings. In particular, sparse time-varying parameter VAR models result by straightforward extensions of the methods discussed in this paper.

The underlying strategy of using the non-centered parametrization of a state space model to extend shrinkage priors introduced for variable selection in regression models to variance selection in a state space model is very generic and many alternative shrinkage priors for variance selection seem worth to be investigated. As pointed out by a reviewer, extending the normal-gamma-gamma prior, introduced recently for highly structured regression models (Griffin and Brown, 2017), to variance selection is a particularly promising venue for future research. This strategy leads to the following “triple gamma prior” in the context of variance selection for state space models for univariate time series:

$$\theta_j | \xi_j^2 \sim \mathcal{G} \left( \frac{1}{2}, \frac{1}{2\xi_j^2} \right), \quad \xi_j^2 | a^\xi, \kappa_j^2 \sim \mathcal{G} (a^\xi, \kappa_j^2/2), \quad \kappa_j^2 \sim \mathcal{G} (c^\xi, d^\xi),$$

with three hyperparameters  $a^\xi$ ,  $c^\xi$ , and  $d^\xi$ . The special case where  $a^\xi = c^\xi = 1/2$  is of particular interest, as it extends the horseshoe prior (Carvalho et al., 2010) to variance selection for state space models which is very popular in regression analysis for its outstanding properties, see e.g. Bhadra et al. (2017).

## Acknowledgements

We are extremely grateful to the Guest Editors Sylvia Kaufmann and Herman van Dijk and two anonymous referees for numerous valuable comments and suggestions that improved the paper considerably. We acknowledge inspiring comments from participants of ESOBE Meetings (Vienna 2012, Oslo 2013, Gerzensee 2015) and NBER-NSF Time Series Conferences (St. Louis 2014, Vienna 2015, New York 2016). We owe special thanks to Mauro Bernardi, discussant of the paper at the 2016 Bolzano Workshop on Forecasting in Finance and Macroeconomics. We are grateful for comments on preliminary versions by participants of CFE 2011, the 1st EFaB Workshop (2013), the 7th Rimini Bayesian Econometrics Workshop (2013), the 1st Vienna Workshop on High Dimensional Time Series in Macroeconomics and Finance (2013), and the 12th ISBA World Meeting (2014).

## References

- Belmonte, M. A. G., Koop, G., and Korobolis, D. (2014). Hierarchical shrinkage in time-varying parameter models. *Journal of Forecasting*, 33:80–94.
- Bhadra, A., Datta, J., Polson, N., and Willard, B. (2017). Lasso meets horseshoe. <https://arxiv.org/abs/1706.10179>.
- Caron, F. and Doucet, A. (2008). Sparse Bayesian nonparametric regression. In McCallum, A. and Roweis, S., editors, *Proceedings of the 25th Annual International Conference on Machine Learning (ICML 2008)*, pages 88–95. Omnipress.
- Carter, C. K. and Kohn, R. (1994). On Gibbs sampling for state space models. *Biometrika*, 81:541–553.
- Carvalho, C. M., Polson, N. G., and Scott, J. G. (2010). The horseshoe estimator for sparse signals. *Biometrika*, 97:465–480.
- Cogley, T., Morozov, S., and Sargent, T. (2005). Bayesian fan charts for U.K. inflation: Forecasting and sources of uncertainty in an evolving monetary system. *Journal of Economic Dynamics and Control*, 16:1893–1925.
- Dangl, T. and Halling, M. (2012). Predictive regressions with time-varying coefficients. *Journal of Financial Economics*, 106:157–181.
- Eisenstat, E., Chan, J. C., and Strachan, R. W. (2014). Stochastic model specification search for time-varying parameter VARs. *SSRN Electronic Journal*, 1.
- Fahrmeir, L., Kneib, T., and Konrath, S. (2010). Bayesian regularisation in structured additive regression: A unifying perspective on shrinkage, smoothing and predictor selection. *Statistics and Computing*, 20:203–219.
- Frühwirth-Schnatter, S. (1992). Approximate predictive integrals for dynamic generalized linear models. In Fahrmeir, L., Francis, B., Gilchrist, R., and Tutz, G., editors, *Advances in GLIM and Statistical Modelling*, number 78 in Lecture Notes in Statistics, pages 123–151. Springer, New York.
- Frühwirth-Schnatter, S. (1994). Data augmentation and dynamic linear models. *Journal of Time Series Analysis*, 15:183–202.
- Frühwirth-Schnatter, S. (1995). Bayesian model discrimination and Bayes factors for linear Gaussian state space models. *Journal of the Royal Statistical Society, Ser. B*, 57:237–246.



- Frühwirth-Schnatter, S. (2004). Efficient Bayesian parameter estimation. In Harvey, A., Koopman, S. J., and Shephard, N., editors, *State Space and Unobserved Component Models: Theory and Applications*, pages 123–151. Cambridge University Press, Cambridge.
- Frühwirth-Schnatter, S. and Tüchler, R. (2008). Bayesian parsimonious covariance estimation for hierarchical linear mixed models. *Statistics and Computing*, 18:1–13.
- Frühwirth-Schnatter, S. and Wagner, H. (2010). Stochastic model specification search for Gaussian and partially non-Gaussian state space models. *Journal of Econometrics*, 154:85–100.
- Frühwirth-Schnatter, S. and Wagner, H. (2011). Bayesian variable selection for random intercept modeling of Gaussian and non-Gaussian data. In Bernardo, J., Bayarri, M., Berger, J., Dawid, A., Heckerman, D., Smith, A., and West, M., editors, *Bayesian Statistics 9*, pages 165–200. Oxford University Press.
- George, E. I. and McCulloch, R. (1993). Variable selection via Gibbs sampling. *Journal of the American Statistical Association*, 88:881–889.
- Geweke, J. and Amisano, G. (2010). Comparing and evaluating Bayesian predictive distributions of asset returns. *International Journal of Forecasting*, 26:216–230.
- Geweke, J. and Jiang, Y. (2011). Inference and prediction in a multiple-structural-break model. *Journal of Econometrics*, 163:172–185.
- Geweke, J. and Keane, M. (2007). Smoothly mixing regressions. *Journal of Econometrics*, 138:252–291.
- Geweke, J. and Tanizaki, H. (1999). On Markov chain Monte Carlo methods for non-linear and non-Gaussian state space models. *Communications in Statistics, Part B – Simulation and Computation*, 28:867–894.
- Gneiting, T. and Raftery, A. (2007). Strictly proper scoring rules, prediction, and estimation. *Journal of the American Statistical Association*, 102:359–378.
- Griffin, J. E. and Brown, P. J. (2010). Inference with normal-gamma prior distributions in regression problems. *Bayesian Analysis*, 5:171–188.
- Griffin, J. E. and Brown, P. J. (2017). Hierarchical shrinkage priors for regression models. *Bayesian Analysis*, 12:135–159.

- Harvey, A. C. (1989). *Forecasting, Structural Time Series Models and the Kalman Filter*. Cambridge University Press, Cambridge.
- Hörmann, W. and Leydold, J. (2014). Generating generalized inverse gaussian random variates. *Statistics and Computing*, 24:547–557.
- Hörmann, W. and Leydold, J. (2015). GIGrvg: Random variate generator for the GIG distribution. R package version 0.4, url: <http://CRAN.R-project.org/package=GIGrvg>.
- Jacquier, E., Polson, N. G., and Rossi, P. E. (1994). Bayesian analysis of stochastic volatility models. *Journal of Business & Economic Statistics*, 12:371–417.
- Kalli, M. and Griffin, J. E. (2014). Time-varying sparsity in dynamic regression models. *Journal of Econometrics*, 178(2):779–793.
- Kastner, G. (2016). Dealing with stochastic volatility in time series using the R package stochvol. *Journal of Statistical Software*, 69:1–30.
- Kastner, G. and Frühwirth-Schnatter, S. (2014). Ancillarity-sufficiency interweaving strategy (ASIS) for boosting MCMC estimation of stochastic volatility models. *Computational Statistics and Data Analysis*, 76:408–423.
- Kastner, G., Frühwirth-Schnatter, S., and Lopes, H. F. (2017). Efficient Bayesian inference for multivariate factor stochastic volatility models. *Journal of Computational and Graphical Statistics*, 26:905–917.
- Lopes, H. F., McCulloch, R. E., and Tsay, R. S. (2016). Parsimony inducing priors for large scale state-space models. *Bayesian Analysis*.
- McCausland, W. J., Miller, S., and Pelletier, D. (2011). Simulation smoothing for state space models: A computational efficiency analysis. *Computational Statistics and Data Analysis*, 55:199–212.
- Mitchell, T. J. and Beauchamp, J. J. (1988). Bayesian variable selection in linear regression. *Journal of the American Statistical Association*, 83:1023–1036.
- Nakajima, J. (2011). Time-varying parameter VAR model with stochastic volatility: An overview of methodology and empirical applications. *Monetary and Economic Studies*, 29:107–142.
- Nakajima, J. and West, M. (2013). Bayesian analysis of latent threshold dynamic models. *Journal of Business & Economic Statistics*, 31:151–164.

- Papaspiliopoulos, O., Roberts, G., and Sköld, M. (2007). A general framework for the parameterization of hierarchical models. *Statistical Science*, 22:59–73.
- Park, T. and Casella, G. (2008). The Bayesian Lasso. *Journal of the American Statistical Association*, 103:681–686.
- Petris, G., Petrone, S., and Campagnoli, P. (2009). *Dynamic Linear Models with R*. Springer, New York.
- Plummer, M., Best, N., Cowles, K., and Vines, K. (2006). CODA: Convergence diagnosis and output analysis for MCMC. *R News*, 6(1):7–11.
- Polson, N. G. and Scott, J. G. (2011). Shrink globally, act locally: Sparse Bayesian regularization and prediction. In Bernardo, J., Bayarri, M., Berger, J., Dawid, A., Heckerman, D., Smith, A., and West, M., editors, *Bayesian Statistics 9*, pages 501–538. Oxford University Press.
- Primiceri, G. (2005). Time varying structural vector autoregressions and monetary policy. *Review of Economic Studies*, 72:821–852.
- Rue, H. and Held, L. (2005). *Gaussian Markov Random Fields: Theory and Applications*, volume 104 of *Monographs on Statistics and Applied Probability*. Chapman & Hall/CRC, London.
- Simpson, M., Niemi, J., and Roy, V. (2017). Interweaving Markov chain Monte Carlo strategies for efficient estimation of dynamic linear models. *Journal of Computational and Graphical Statistics*, 26:152–159.
- Sims, C. A. (2001). [Evolving post-world war II US inflation dynamics]: Comment. *NBER Macroeconomics Annual*, 16:373–379.
- Stock, J. H. and Watson, M. W. (2012). Generalized shrinkage methods for forecasting using many predictors. *Journal of Business & Economic Statistics*, 30(4):481–493.
- West, M. and Harrison, P. J. (1997). *Bayesian Forecasting and Dynamic Models*. Springer, New York, 2 edition.
- Yu, Y. and Meng, X.-L. (2011). To center or not to center: that is not the question - an ancillarity-sufficiency interweaving strategy (ASIS) for boosting MCMC efficiency. *Journal of Computational and Graphical Statistics*, 20(3):531–570.
- Zhao, Z. Y., Xie, M., and West, M. (2016). Dynamic dependence networks: Financial time series forecasting and portfolio decisions. *Applied Stochastic Models in Business and Industry*, 32:311–332.

# Achieving Shrinkage in a Time-Varying Parameter Model Framework Webappendix

Angela Bitto and Sylvia Frühwirth-Schnatter

Institute for Statistics and Mathematics  
Department of Finance, Accounting and Statistics  
WU Vienna University of Economics and Business, Vienna, Austria  
Email: `angela.bitto@wu.ac.at`, `sfruehwi@wu.ac.at`

## A.1 Computational Details

### A.1.1 Details on the MCMC scheme in Algorithm 1

#### A.1.1.1 Step (a): Sampling the latent states

Step (a) of Algorithm 1 samples the latent states  $\tilde{\boldsymbol{\beta}} = (\tilde{\boldsymbol{\beta}}_0, \tilde{\boldsymbol{\beta}}_1, \dots, \tilde{\boldsymbol{\beta}}_T)$  conditional on known parameters using either *Forward Filtering Backward Sampling* (FFBS), as discussed in Frühwirth-Schnatter (1994) and Carter and Kohn (1994), or the faster alternative known as *all without a loop* (AWOL), discussed in McCausland et al. (2011) and Kastner and Frühwirth-Schnatter (2014). Subsequently, we provide details how the AWOL algorithm is implemented for TVP models.

The algorithm is implemented for a slight modification of the non-centered TVP model (7) and (9), given by:

$$\begin{aligned}\tilde{\beta}_{jt} &= \tilde{\beta}_{j,t-1} + \tilde{\omega}_{jt}, & \tilde{\omega}_{jt} &\sim \mathcal{N}(0, 1), \\ y_t^* &= \mathbf{F}_t \tilde{\boldsymbol{\beta}}_t + \varepsilon_t, & \varepsilon_t &\sim \mathcal{N}(0, \sigma_t^2),\end{aligned}$$

with outcome  $y_t^* = y_t - \mathbf{x}_t \boldsymbol{\beta}$  and  $\mathbf{F}_t = \mathbf{x}_t \text{Diag}(\sqrt{\theta_1}, \dots, \sqrt{\theta_d})$  for  $t = 1, \dots, T$ . The homoscedastic model results with  $\sigma_1^2 = \dots = \sigma_T^2 = \sigma^2$ .

Conditional on all other variables, the joint density for the state process  $\tilde{\boldsymbol{\beta}} = (\tilde{\boldsymbol{\beta}}_0, \tilde{\boldsymbol{\beta}}_1, \dots, \tilde{\boldsymbol{\beta}}_T)$  is multivariate normal. This distribution can be written in terms of the tri-diagonal precision matrix  $\boldsymbol{\Omega}$  and the covector  $\mathbf{c}$ , see also Rue and Held (2005):

$$\tilde{\boldsymbol{\beta}} | \boldsymbol{\beta}, \mathbf{Q}, \mathbf{P}_0, \sigma^2 \sim \mathcal{N}_{(T+1)d}(\boldsymbol{\Omega}^{-1} \mathbf{c}, \boldsymbol{\Omega}^{-1}), \quad (\text{A.1})$$

where:

$$\mathbf{\Omega} = \begin{bmatrix} \mathbf{\Omega}_{00} & \mathbf{\Omega}_{01} & 0 & & & \\ \mathbf{\Omega}'_{01} & \mathbf{\Omega}_{11} & \mathbf{\Omega}_{12} & 0 & 0 & \\ 0 & \mathbf{\Omega}'_{12} & \mathbf{\Omega}_{22} & \mathbf{\Omega}_{23} & \ddots & \vdots \\ & 0 & \mathbf{\Omega}'_{23} & \ddots & \ddots & 0 \\ & \vdots & \ddots & \ddots & \mathbf{\Omega}_{T-1,T-1} & \mathbf{\Omega}_{T-1,T} \\ 0 & \dots & 0 & \mathbf{\Omega}'_{T-1,T} & \mathbf{\Omega}_{TT} \end{bmatrix}, \quad \mathbf{c} = \begin{bmatrix} \mathbf{c}_0 \\ \mathbf{c}_1 \\ \mathbf{c}_2 \\ \vdots \\ \mathbf{c}_T \end{bmatrix}.$$

In this representation, each submatrix  $\mathbf{\Omega}_{ts}$  is a matrix of dimension  $d \times d$  defined as

$$\begin{aligned} \mathbf{\Omega}_{00} &= \text{Diag}(1/P_{0,11} \cdots 1/P_{0,dd}) + \mathbf{I}_d, \\ \mathbf{\Omega}_{tt} &= \mathbf{F}'_t \mathbf{F}_t / \sigma_t^2 + 2\mathbf{I}_d, \quad t = 1, \dots, T-1, \\ \mathbf{\Omega}_{TT} &= \mathbf{F}'_T \mathbf{F}_T / \sigma_T^2 + \mathbf{I}_d, \\ \mathbf{\Omega}_{t,t+1} &= -\mathbf{I}_d, \quad t = 0, \dots, T-1, \end{aligned}$$

where  $\mathbf{I}_d$  is the  $d \times d$  identity matrix and  $\mathbf{c}_t$  is a column vector of dimension  $d \times 1$ , defined as

$$\mathbf{c}_0 = \mathbf{0}, \quad \mathbf{c}_t = (\mathbf{F}'_t / \sigma_t^2) y_t^*, \quad t = 1, \dots, T.$$

The specific structure of  $\mathbf{\Omega}$  allows sampling the state process  $\tilde{\boldsymbol{\beta}} = (\tilde{\boldsymbol{\beta}}_0, \dots, \tilde{\boldsymbol{\beta}}_T)$ , *all without a loop* from the  $(T+1)d$ -variate normal posterior distribution  $\tilde{\boldsymbol{\beta}} | \boldsymbol{\beta}, \mathbf{Q}, \mathbf{P}_0, \sigma^2 \sim \mathcal{N}_{(T+1)d}(\mathbf{\Omega}^{-1} \mathbf{c}, \mathbf{\Omega}^{-1})$ . Due to the band structure of  $\mathbf{\Omega}$ , calculating the Cholesky decomposition  $\mathbf{\Omega} = \mathbf{L}\mathbf{L}'$  is computationally inexpensive. Based on a draw  $\boldsymbol{\epsilon} \sim \mathcal{N}_{(T+1)d}(\mathbf{0}, \mathbf{I})$ , we solve  $\mathbf{L}\mathbf{a} = \mathbf{c}$  for  $\mathbf{a}$  and  $\mathbf{L}'\tilde{\boldsymbol{\beta}} = \mathbf{a} + \boldsymbol{\epsilon}$  for  $\tilde{\boldsymbol{\beta}}$  by using back-band substitution instead of actually calculating  $\mathbf{L}^{-1}$ . Further details on this method can be found in McCausland et al. (2011).

#### A.1.1.2 Step (b): Sampling the constant coefficients $\beta_j$ and the square root of the process variances $\sqrt{\theta_j}$

Conditional on the state process  $\tilde{\boldsymbol{\beta}} = (\tilde{\boldsymbol{\beta}}_0, \tilde{\boldsymbol{\beta}}_1, \dots, \tilde{\boldsymbol{\beta}}_T)$ , the observation equation (9) of the non-centered state space model defines an expanded regression model:

$$y_t = \mathbf{z}_t \boldsymbol{\alpha} + \varepsilon_t, \quad \varepsilon_t \sim \mathcal{N}(0, \sigma_t^2),$$

with regression coefficient  $\boldsymbol{\alpha} = (\beta_1, \dots, \beta_d, \sqrt{\theta_1}, \dots, \sqrt{\theta_d})'$  and covariate vector  $\mathbf{z}_t$  defined as:

$$\mathbf{z}_t = \begin{pmatrix} x_{t1} & \cdots & x_{td} & x_{t1}\tilde{\beta}_{1t} & \cdots & x_{td}\tilde{\beta}_{dt} \end{pmatrix}. \quad (\text{A.2})$$

Under the conjugate prior  $\boldsymbol{\alpha}|\boldsymbol{\tau}, \boldsymbol{\xi} \sim \mathcal{N}_{2d}(\mathbf{0}, \mathbf{A}_0)$ , where  $\mathbf{A}_0 = \text{Diag}(\tau_1^2, \dots, \tau_d^2, \xi_1^2, \dots, \xi_d^2)$ , it follows that the conditional posterior distribution  $p(\boldsymbol{\alpha}|\tilde{\boldsymbol{\beta}}, \boldsymbol{\tau}, \boldsymbol{\xi}, \sigma_1^2, \dots, \sigma_T^2, \mathbf{y})$  is a multivariate normal distribution,

$$\boldsymbol{\alpha}|\tilde{\boldsymbol{\beta}}, \boldsymbol{\tau}, \boldsymbol{\xi}, \sigma_1^2, \dots, \sigma_T^2, \mathbf{y} \sim \mathcal{N}_{2d}(\mathbf{a}_T, \mathbf{A}_T), \quad (\text{A.3})$$

with

$$\mathbf{a}_T = \mathbf{A}_T \tilde{\mathbf{W}} \mathbf{y}, \quad \mathbf{A}_T = \left( \tilde{\mathbf{W}} \mathbf{W} + \mathbf{A}_0^{-1} \right)^{-1},$$

where  $\mathbf{y} = (y_1, \dots, y_T)'$  and  $\mathbf{W}$  is a  $(T \times 2d)$  regressor matrix with the  $t$ -th row being equal to  $\mathbf{z}_t$  and  $\tilde{\mathbf{W}} = \mathbf{W}' \text{Diag}(1/\sigma_1^2, \dots, 1/\sigma_T^2)$ .

In a shrinkage framework, some of the variances  $\tau_j^2$  and  $\xi_j^2$  may be close to zero, leading to conditional priors  $p(\beta_j|\tau_j^2)$  and  $p(\sqrt{\theta_j}|\xi_j^2)$  with huge prior information equal to  $1/\tau_j^2$  and  $1/\xi_j^2$ . In order to overcome numerical difficulties with such very informative priors, we make use of the following alternative computation of the posterior covariance matrix  $\mathbf{A}_T$ :

$$\mathbf{A}_T = \mathbf{A}_0^{1/2} \mathbf{A}_T^* \mathbf{A}_0^{1/2},$$

$$\mathbf{A}_0^{1/2} = \text{Diag}(\tau_1, \dots, \tau_d, \xi_1, \dots, \xi_d), \quad \mathbf{A}_T^* = \left( \mathbf{A}_0^{1/2} \tilde{\mathbf{W}} \mathbf{W} \mathbf{A}_0^{1/2} + \mathbf{I}_{2d} \right)^{-1}.$$

### A.1.1.3 Step (c): Sampling the prior variances

For the normal-gamma hierarchical priors given in (12) and (17), it follows that the conditionally normal prior  $\beta_j|\tau_j^2 (\sqrt{\theta_j}|\xi_j^2)$  leads to a posterior for the variance  $\tau_j^2|\beta_j, a^\tau, \lambda^2 (\xi_j^2|\theta_j, a^\xi, \kappa^2)$ , where the likelihood is the kernel of an inverted gamma density in  $\tau_j^2 (\xi_j^2)$ . In combination with the gamma prior  $\tau_j^2|a^\tau, \lambda^2 \sim \mathcal{G}(a^\tau, a^\tau \lambda^2/2)$  ( $\xi_j^2|a^\xi, \kappa^2 \sim \mathcal{G}(a^\xi, a^\xi \kappa^2/2)$ ), this leads to a generalized inverse Gaussian distribution for  $\tau_j^2|\beta_j, a^\tau, \lambda^2 (\xi_j^2|\theta_j, a^\xi, \kappa^2)$ :

$$\tau_j^2|\beta_j, a^\tau, \lambda^2 \sim \mathcal{GIG}(a^\tau - 1/2, a^\tau \lambda^2, \beta_j^2), \quad (\text{A.4})$$

$$\xi_j^2|\theta_j, a^\xi, \kappa^2 \sim \mathcal{GIG}(a^\xi - 1/2, a^\xi \kappa^2, \theta_j). \quad (\text{A.5})$$

The generalized inverse Gaussian distribution,  $Y \sim \mathcal{GIG}(p, a, b)$ ,  $a > 0, b > 0$  is a three parameter family with support on  $y \in \mathbb{R}^+$ . The density is given by

$$f(y) = \frac{(a/b)^{p/2}}{2K_p(\sqrt{ab})} y^{p-1} e^{-(a/2)y} e^{-b/(2y)},$$

where  $K_p(\cdot)$  is the modified Bessel function of the second kind. The  $k$ th moment  $\mu_k = E(Y^k)$  is given as

$$\mu_k = \frac{K_{p+k}(\sqrt{ab})}{K_p(\sqrt{ab})} \left( \sqrt{\frac{b}{a}} \right)^k.$$

Hörmann and Leydold (2014) propose a new generation method for the cases where  $p < 1$ ,  $\sqrt{ab} < 0.5$ , which is especially useful in the time-varying parameter case. A very stable generator is implemented in the R-package **GIGrvg** (Hörmann and Leydold, 2015).

As we have equipped  $\lambda^2$  and  $\kappa^2$  with hyperpriors  $\lambda^2 \sim \mathcal{G}(e_1, e_2)$  and  $\kappa^2 \sim \mathcal{G}(d_1, d_2)$ , we need to sample these parameters from the corresponding conditional posteriors:

$$\lambda^2 | a^\tau, \tau_1^2, \dots, \tau_d^2 \sim \mathcal{G} \left( e_1 + a^\tau d, e_2 + \frac{\overline{\tau^2}}{2} a^\tau d \right), \quad (\text{A.6})$$

$$\kappa^2 | a^\xi, \xi_1^2, \dots, \xi_d^2 \sim \mathcal{G} \left( d_1 + a^\xi d, d_2 + \frac{\overline{\xi^2}}{2} a^\xi d \right), \quad (\text{A.7})$$

where  $\overline{\tau^2}$  and  $\overline{\xi^2}$  are the averages of the variances in the shrinkage priors:

$$\overline{\tau^2} = \frac{1}{d} \sum_{j=1}^d \tau_j^2, \quad \overline{\xi^2} = \frac{1}{d} \sum_{j=1}^d \xi_j^2.$$

If  $\overline{\xi^2}$  is small, i.e. a lot of sparsity is present, then the posterior expectation of  $\kappa^2$  will be proportional to  $1/d_2$ . Hence, smaller values of  $d_2$  encourage stronger prior shrinkage of  $\theta_j$  toward zero.

## A.1.2 Approximating the one-step ahead predictive density

### A.1.2.1 Using the Kalman filter for prediction for known parameters

It is well-known that the Kalman filter can be applied to derive the predictive density in a Gaussian state space model for known model parameters. We exploit this procedure to derive the predictive density  $p(y_t | \mathbf{y}^{t-1}, \boldsymbol{\beta}, \mathbf{Q}, \sigma_t^2)$  for known values of the parameters  $\boldsymbol{\beta}$ ,  $\mathbf{Q}$ , and  $\sigma_t^2$ , given observations  $\mathbf{y}^{t-1} = (y_1, \dots, y_{t-1})$ . In the following, details are provided for the non-centered parameterization of the TVP model, based on rewriting the observation equation (9) as:

$$\begin{aligned} \tilde{\boldsymbol{\beta}}_t &= \tilde{\boldsymbol{\beta}}_{t-1} + \tilde{\boldsymbol{\omega}}_t, \quad \tilde{\boldsymbol{\omega}}_t \sim \mathcal{N}(0, \mathbf{I}_d), \\ y_t &= \mathbf{x}_t \boldsymbol{\beta} + \mathbf{F}_t \tilde{\boldsymbol{\beta}}_t + \varepsilon_t, \quad \varepsilon_t \sim \mathcal{N}(0, \sigma_t^2), \end{aligned}$$

where  $\mathbf{F}_t = \mathbf{x}_t \text{Diag}(\sqrt{\theta_1}, \dots, \sqrt{\theta_d})$ . Starting from  $\tilde{\boldsymbol{\beta}}_0 \sim \mathcal{N}_d(\mathbf{m}_0, \mathbf{C}_0)$  with  $\mathbf{m}_0 = \mathbf{0}$  and  $\mathbf{C}_0 = \mathbf{P}_0 = \text{Diag}(P_{0,11} \cdots P_{0,dd})$ , the following three steps are repeated for  $t = 1, \dots, T - 1$ :<sup>17</sup>

(a) A *propagation step* to determine the one-step ahead predictive density  $p(\tilde{\boldsymbol{\beta}}_t | \mathbf{y}^{t-1})$ :

$$\begin{aligned}\tilde{\boldsymbol{\beta}}_t | \mathbf{y}^{t-1} &\sim \mathcal{N}_d(\mathbf{m}_{t-1}, \mathbf{R}_t), \\ \mathbf{R}_t &= \mathbf{C}_{t-1} + \mathbf{I}_d.\end{aligned}$$

(b) A *prediction step* to determine the predictive density  $p(y_t | \mathbf{y}^{t-1})$ :

$$\begin{aligned}y_t | \mathbf{y}^{t-1} &\sim \mathcal{N}(\hat{y}_t, S_t), \\ \hat{y}_t &= \mathbf{x}_t \boldsymbol{\beta} + \mathbf{F}_t \mathbf{m}_{t-1}, \quad S_t = \mathbf{F}_t \mathbf{R}_t \mathbf{F}_t' + \sigma_t^2.\end{aligned}$$

(c) A *correction step* to determine the filter density  $p(\tilde{\boldsymbol{\beta}}_t | \mathbf{y}^t)$ :

$$\begin{aligned}\tilde{\boldsymbol{\beta}}_t | \mathbf{y}^t &\sim \mathcal{N}_d(\mathbf{m}_t, \mathbf{C}_t), \\ \mathbf{m}_t &= \mathbf{m}_{t-1} + \mathbf{K}_t(y_t - \hat{y}_t), \quad \mathbf{K}_t = \mathbf{R}_t \mathbf{F}_t' S_t^{-1}, \quad \mathbf{C}_t = (\mathbf{I}_d - \mathbf{K}_t \mathbf{F}_t) \mathbf{R}_t.\end{aligned}$$

Note that prediction could equally well be performed in the centered parametrization of the TVP model.

#### A.1.2.2 Approximations for the one-step ahead predictive density in a TVP model

In Section 4, the conditionally optimal Kalman mixture approximation was introduced to approximate the one-step ahead predictive density  $p(y_t | \mathbf{y}^{t-1})$ . As it performs *exact* analytical integration with respect to the entire state process  $\tilde{\boldsymbol{\beta}}_0, \dots, \tilde{\boldsymbol{\beta}}_t$ , not surprisingly, we found that this method outperforms alternative approximations.

Belmonte et al. (2014), for instance, employ a purely simulation-based approach to approximate  $p(y_t | \mathbf{y}^{t-1})$  in a univariate framework. Based on the same output of the Gibbs sampler as the conditionally optimal Kalman mixture approximation, they derive draws from the predictive density by using following simulation method suggested in Cogley et al. (2005, Section 2.1). More specifically, for each posterior draw  $m = 1, \dots, M$ , generate  $\tilde{\beta}_{jt}^{(m)}$  by drawing from the normal distribution  $\mathcal{N}(\tilde{\beta}_{j,t-1}^{(m)}, 1)$  and transform to generate  $\beta_{jt}^{(m)} = \beta_j^{(m)} + \sqrt{\theta_j^{(m)}} \tilde{\beta}_{jt}^{(m)}$  for all  $j = 1, \dots, d$ . Based on  $\boldsymbol{\beta}_t^{(m)} = (\beta_{1t}^{(m)}, \dots, \beta_{dt}^{(m)})'$ , forecast

---

<sup>17</sup>To simplify the notation, dependence on the model parameters  $\boldsymbol{\beta}, \mathbf{Q}$ , and  $\sigma_1^2, \dots, \sigma_T^2$  is not made explicit.



a future value  $y_t^{(m)}$  by drawing from  $p(y_t|\boldsymbol{\beta}_t^{(m)}, \sigma_t^{2(m)})$ :

$$y_t^{(m)} = \mathbf{x}_t \boldsymbol{\beta}_t^{(m)} + \varepsilon_t^{(m)}, \quad \varepsilon_t^{(m)} \sim \mathcal{N}\left(0, \sigma_t^{2(m)}\right).$$

The same method as in Section 4 is applied to forecast  $\sigma_t^{2(m)}$  for the SV specification. Finally, for each time point  $t$ , Belmonte et al. (2014) perform a nonparametric kernel smoothing algorithm on  $y_t^{(m)}$  for  $m = 1, \dots, M$ , which is then evaluated at the observed value  $y_t$ . To this aim, they use the function `ksdensity` in Matlab, which returns a probability density estimate evaluated at the observed value  $y_t$ . This approximation method is expected to be rather inaccurate in a multivariate setting, where the scores  $\text{LPDS}_{i,t}^*$  are approximated individually for each time series and aggregated through (29) to obtain  $\text{LPDS}_t^*$  and approximation errors easily accumulate.

We also experimented with what we call the *naive Gaussian mixture approximation*. This approximation is based on choosing  $\boldsymbol{\vartheta} = (\boldsymbol{\beta}_t, \sigma_t^2)$  in the mixture approximation (21) and using the predictive density  $y_t|\boldsymbol{\beta}_t, \sigma_t^2 \sim \mathcal{N}(\mathbf{x}_t \boldsymbol{\beta}_t, \sigma_t^2)$  as component density. The parameters  $\boldsymbol{\vartheta}^{(m)} = (\boldsymbol{\beta}_t^{(m)}, \sigma_t^{2(m)})$  are sampled from the predictive posterior distribution  $p(\boldsymbol{\beta}_t, \sigma_t^2 | \mathbf{y}^{t-1})$  as in Belmonte et al. (2014). This yields

$$\begin{aligned} p(y_t | \mathbf{y}^{t-1}) &= \int p(y_t | \boldsymbol{\beta}_t, \sigma_t^2) p(\boldsymbol{\beta}_t, \sigma_t^2 | \mathbf{y}^{t-1}) d(\boldsymbol{\beta}_t, \sigma_t^2) \\ &\approx \frac{1}{M} \sum_{m=1}^M f_N\left(y_t; \mathbf{x}_t \boldsymbol{\beta}_t^{(m)}, (\sigma_t^2)^{(m)}\right). \end{aligned} \quad (\text{A.8})$$

Whereas the naive Gaussian mixture approximation (A.8) avoids kernel density estimation, it can give very imprecise results, in particular for state space models with a high signal-to-noise ratio. This occurs, when the error variance  $(\sigma_t^2)^{(m)}$  is considerably smaller than the forecasting variance  $S_t^{(m)}$  in the conditionally optimal Kalman filter approximation (22), see Frühwirth-Schnatter (1992) for an early discussion of this problem and Section A.3.2 for more empirical details.

## A.2 Data description

### A.2.1 ECB data

The inflation data analyzed in Section 7.1 can be retrieved freely from the ECB data warehouse.<sup>18</sup> The data are monthly and range from February 1994 until November 2010. The time series are listed in Table A.1 and plotted in Figure A.1. The original time series

<sup>18</sup>For details and data see <http://sdw.ecb.europa.eu/>.

$i$	Symbol	Description
1	I-1MO	one-month Euribor (Euro interbank offered rate)
2	I-1YR	one-year Euribor (Euro interbank offered rate)
3	SENT	percentage change in economic sentiment indicator
4	STOCK-1	percentage change in equity index (Dow Jones, Euro Stoxx, Economic sector index financial)
5	STOCK-2	percentage change in equity index - Dow Jones Euro Stoxx 50 index
6	EXRATE	percentage change in ECB real effective exchange rate (CPI deflated, broad group of currencies against euro)
7	IP	percentage change in industrial production index
8	LOANS	percentage change in loans (total maturity, all currencies combined)
9	M3	annual percentage change in monetary aggregate M3
10	CAR	registrations of new passenger cars
11	OIL	percentage change in oil price (brent crude, 1-month forward)
12	ORDER	change in order-book levels
13	UNEMP	standardized unemployment rate (all ages, male & female)
14	HICP	harmonized index of consumer prices

Table A.1: ECB data. Data description.

were transformed (log differences, differences) as in Belmonte et al. (2014) and each of the time series was standardized. The core inflation rate was transformed to have variance one.

### A.2.2 DAX data

The DAX - Deutscher Aktienindex (German stock index) is a blue chip stock market index consisting of the 30 major German companies trading on the Frankfurt Stock Exchange, see Table A.2. The data set analyzed in Section 7.2 spans roughly 2500 daily stock returns from September 4th, 2001 until August 31st, 2011. One of the companies was excluded from the case study, as it was not part of the DAX for the entire observation period.

## A.3 Further results

### A.3.1 Detailed estimation results for the ECB data

Table A.3 summarizes the posterior distributions  $p(\beta_j|\mathbf{y})$  and  $p(\sqrt{\theta_j}|\mathbf{y})$  for  $j = 1, \dots, 37$ , for the EU-area inflation data analyzed in Section 7.1.

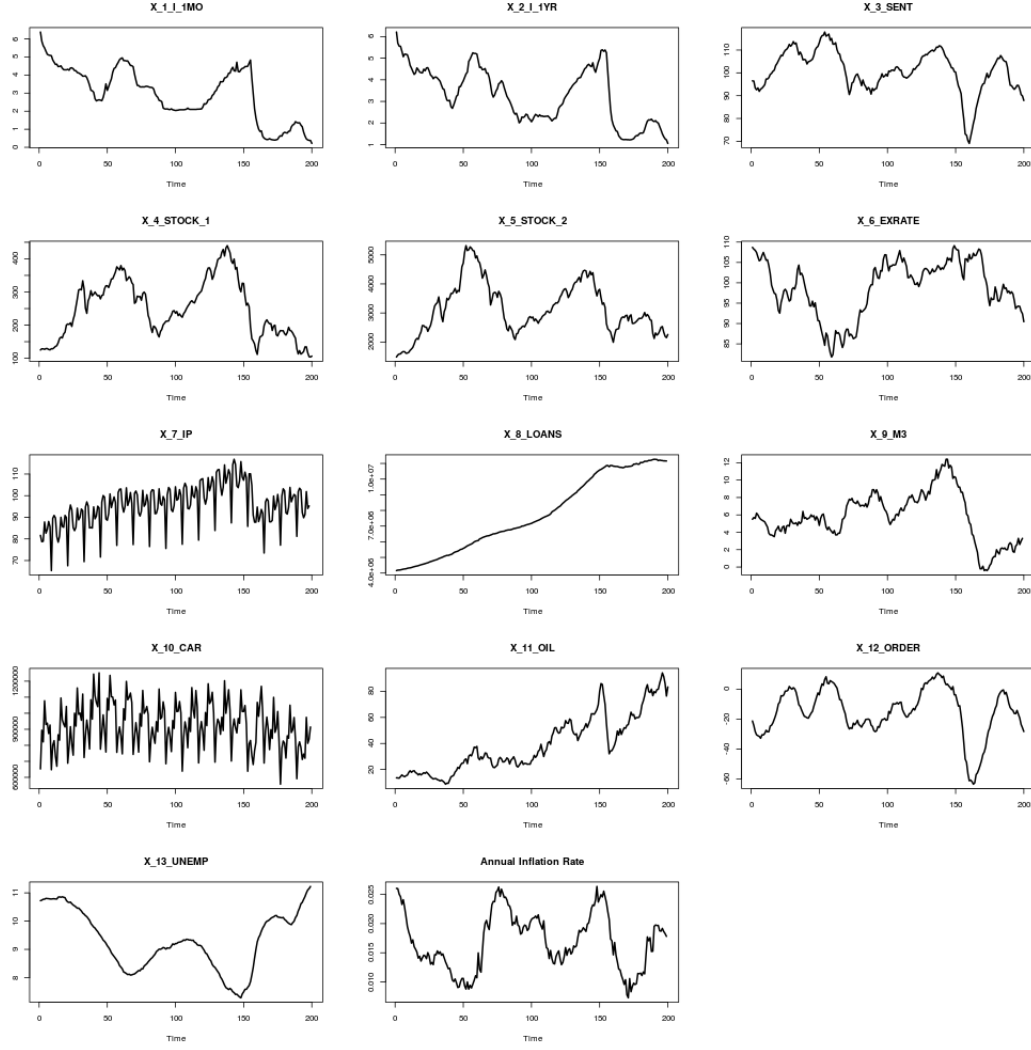


Figure A.1: ECB data. Original time series.

	Covariate	Mean	Stdev.	Median	2.5% quantil	97.5% quantil
$\beta_1$	Intercept	2.770	0.655	2.782	1.450	4.016
$\beta_2$	$\pi_t$	$1.8 \cdot 10^{-3}$	0.021	$3.8 \cdot 10^{-5}$	-0.039	0.049
$\beta_3$	$\pi_{t-1}$	$-3.7 \cdot 10^{-3}$	0.012	$-3.4 \cdot 10^{-4}$	-0.051	0.033
$\beta_4$	$\pi_{t-2}$	$-9.1 \cdot 10^{-3}$	0.021	$-2.3 \cdot 10^{-3}$	-0.063	0.023
$\beta_5$	$\pi_{t-3}$	$-4.1 \cdot 10^{-4}$	0.018	$9.2 \cdot 10^{-8}$	-0.040	0.037
$\beta_6$	$\pi_{t-4}$	$-3.6 \cdot 10^{-3}$	0.019	$-3.4 \cdot 10^{-4}$	-0.050	0.033
$\beta_7$	$\pi_{t-5}$	0.019	0.027	0.010	-0.017	0.084
$\beta_8$	$\pi_{t-6}$	$1.5 \cdot 10^{-3}$	0.018	$6.0 \cdot 10^{-5}$	-0.036	0.043
$\beta_9$	$\pi_{t-7}$	$-9.2 \cdot 10^{-3}$	0.023	$-2.0 \cdot 10^{-3}$	-0.068	0.025
$\beta_{10}$	$\pi_{t-8}$	$-1.2 \cdot 10^{-3}$	0.021	$-3.9 \cdot 10^{-5}$	-0.049	0.043
$\beta_{11}$	$\pi_{t-9}$	-0.010	0.025	$-1.9 \cdot 10^{-3}$	-0.079	0.026

*Continued on next page*

Table A.3 – *Continued from previous page*

	Name	Mean	Stdev.	Median	2.5% quantil	97.5% quantil
$\beta_{12}$	$\pi_{t-10}$	$-4.6 \cdot 10^{-3}$	0.022	$-2.5 \cdot 10^{-4}$	-0.062	0.032
$\beta_{13}$	$\pi_{t-11}$	-0.041	0.047	-0.030	-0.150	0.020
$\beta_{14}$	I-1MO	0.595	0.259	0.586	0.078	1.130
$\beta_{15}$	I-1YR	0.152	0.245	0.052	-0.172	0.774
$\beta_{16}$	SENT	$-6.9 \cdot 10^{-3}$	0.021	$-1.6 \cdot 10^{-3}$	-0.056	0.029
$\beta_{17}$	STOCK-1	0.024	0.032	0.015	-0.018	0.104
$\beta_{18}$	STOCK-2	$-1.2 \cdot 10^{-3}$	0.028	$2.8 \cdot 10^{-6}$	-0.068	0.054
$\beta_{19}$	EXRATE	$4.5 \cdot 10^{-3}$	0.018	$9.3 \cdot 10^{-4}$	-0.028	0.043
$\beta_{20}$	IP	$2.0 \cdot 10^{-3}$	0.012	$2.3 \cdot 10^{-4}$	-0.022	0.030
$\beta_{21}$	LOANS	$-1.0 \cdot 10^{-3}$	0.017	$-4.9 \cdot 10^{-5}$	-0.038	0.033
$\beta_{22}$	M3	-0.079	0.251	-0.011	-0.720	0.295
$\beta_{23}$	CAR	$4.2 \cdot 10^{-3}$	0.028	$1.2 \cdot 10^{-3}$	-0.056	0.060
$\beta_{24}$	OIL	$-4.2 \cdot 10^{-3}$	0.014	$-7.1 \cdot 10^{-4}$	-0.039	0.021
$\beta_{25}$	ORDER	$3.8 \cdot 10^{-3}$	0.021	$1.9 \cdot 10^{-4}$	-0.030	0.054
$\beta_{26}$	UNEMP	0.261	0.428	0.078	-0.255	1.387
$\beta_{27}$	$D_{t,1}$	$-4.6 \cdot 10^{-3}$	0.044	$-4.9 \cdot 10^{-4}$	-0.104	0.087
$\beta_{28}$	$D_{t,2}$	$-7.5 \cdot 10^{-3}$	0.048	$-3.7 \cdot 10^{-4}$	-0.127	0.082
$\beta_{29}$	$D_{t,3}$	0.022	0.055	$7.2 \cdot 10^{-3}$	-0.074	0.153
$\beta_{30}$	$D_{t,4}$	0.026	0.051	$7.8 \cdot 10^{-3}$	-0.048	0.155
$\beta_{31}$	$D_{t,5}$	0.014	0.044	$2.4 \cdot 10^{-3}$	-0.065	0.124
$\beta_{32}$	$D_{t,6}$	-0.012	0.043	$-1.7 \cdot 10^{-3}$	-0.122	0.067
$\beta_{33}$	$D_{t,7}$	-0.026	0.053	$-6.5 \cdot 10^{-3}$	-0.163	0.052
$\beta_{34}$	$D_{t,8}$	$2.3 \cdot 10^{-3}$	0.040	$9.0 \cdot 10^{-5}$	-0.086	0.097
$\beta_{35}$	$D_{t,9}$	$-4.9 \cdot 10^{-4}$	0.039	$5.3 \cdot 10^{-6}$	-0.091	0.086
$\beta_{36}$	$D_{t,10}$	$-3.3 \cdot 10^{-3}$	0.040	$-1.0 \cdot 10^{-4}$	-0.099	0.081
$\beta_{37}$	$D_{t,11}$	0.061	0.073	0.042	-0.037	0.231
$ \sqrt{\theta_1} $	Intercept	0.166	0.027	0.168	0.106	0.213
$ \sqrt{\theta_2} $	$\pi_t$	$9.8 \cdot 10^{-4}$	$2.1 \cdot 10^{-3}$	$1.2 \cdot 10^{-4}$	$2.1 \cdot 10^{-8}$	$7.2 \cdot 10^{-3}$
$ \sqrt{\theta_3} $	$\pi_{t-1}$	$9.0 \cdot 10^{-4}$	$2.0 \cdot 10^{-3}$	$1.2 \cdot 10^{-4}$	$2.2 \cdot 10^{-8}$	$6.3 \cdot 10^{-3}$
$ \sqrt{\theta_4} $	$\pi_{t-2}$	$8.8 \cdot 10^{-4}$	$1.8 \cdot 10^{-3}$	$1.2 \cdot 10^{-4}$	$2.0 \cdot 10^{-8}$	$6.1 \cdot 10^{-3}$
$ \sqrt{\theta_5} $	$\pi_{t-3}$	$7.8 \cdot 10^{-4}$	$1.6 \cdot 10^{-3}$	$1.1 \cdot 10^{-4}$	$2.1 \cdot 10^{-8}$	$5.4 \cdot 10^{-3}$
$ \sqrt{\theta_6} $	$\pi_{t-4}$	$9.7 \cdot 10^{-4}$	$1.9 \cdot 10^{-3}$	$1.4 \cdot 10^{-4}$	$2.1 \cdot 10^{-8}$	$6.7 \cdot 10^{-3}$
$ \sqrt{\theta_7} $	$\pi_{t-5}$	$9.0 \cdot 10^{-4}$	$1.8 \cdot 10^{-3}$	$1.3 \cdot 10^{-4}$	$2.2 \cdot 10^{-8}$	$6.2 \cdot 10^{-3}$
$ \sqrt{\theta_8} $	$\pi_{t-6}$	$7.6 \cdot 10^{-4}$	$1.5 \cdot 10^{-3}$	$1.1 \cdot 10^{-4}$	$2.0 \cdot 10^{-8}$	$5.2 \cdot 10^{-3}$
$ \sqrt{\theta_9} $	$\pi_{t-7}$	$9.6 \cdot 10^{-4}$	$2.1 \cdot 10^{-3}$	$1.2 \cdot 10^{-4}$	$2.2 \cdot 10^{-8}$	$6.8 \cdot 10^{-3}$
$ \sqrt{\theta_{10}} $	$\pi_{t-8}$	$1.1 \cdot 10^{-3}$	$2.5 \cdot 10^{-3}$	$1.3 \cdot 10^{-4}$	$2.0 \cdot 10^{-8}$	$7.8 \cdot 10^{-3}$
$ \sqrt{\theta_{11}} $	$\pi_{t-9}$	$8.7 \cdot 10^{-4}$	$1.8 \cdot 10^{-3}$	$1.1 \cdot 10^{-4}$	$1.8 \cdot 10^{-8}$	$6.1 \cdot 10^{-3}$
$ \sqrt{\theta_{12}} $	$\pi_{t-10}$	$8.3 \cdot 10^{-4}$	$1.7 \cdot 10^{-3}$	$1.2 \cdot 10^{-4}$	$2.1 \cdot 10^{-8}$	$5.8 \cdot 10^{-3}$

*Continued on next page*

Table A.3 – *Continued from previous page*

	Name	Mean	Stdev.	Median	2.5% quantil	97.5% quantil
$ \sqrt{\theta}_{13} $	$\pi_{t-11}$	$1.6 \cdot 10^{-3}$	$3.0 \cdot 10^{-3}$	$2.1 \cdot 10^{-4}$	$2.5 \cdot 10^{-8}$	0.011
$ \sqrt{\theta}_{14} $	I_1MO	0.019	0.027	$3.6 \cdot 10^{-3}$	$5.2 \cdot 10^{-8}$	0.091
$ \sqrt{\theta}_{15} $	I_1YR	0.026	0.028	0.018	$1.1 \cdot 10^{-7}$	0.092
$ \sqrt{\theta}_{16} $	SENT	$1.2 \cdot 10^{-3}$	$2.7 \cdot 10^{-3}$	$1.6 \cdot 10^{-4}$	$2.2 \cdot 10^{-8}$	$9.0 \cdot 10^{-3}$
$ \sqrt{\theta}_{17} $	STOCK1	$1.4 \cdot 10^{-3}$	$2.7 \cdot 10^{-3}$	$1.8 \cdot 10^{-4}$	$2.3 \cdot 10^{-8}$	$9.3 \cdot 10^{-3}$
$ \sqrt{\theta}_{18} $	STOCK2	$1.6 \cdot 10^{-3}$	$3.2 \cdot 10^{-3}$	$2.0 \cdot 10^{-4}$	$2.4 \cdot 10^{-8}$	0.011
$ \sqrt{\theta}_{19} $	EXRATE	$1.2 \cdot 10^{-3}$	$2.4 \cdot 10^{-3}$	$1.5 \cdot 10^{-4}$	$2.1 \cdot 10^{-8}$	$8.1 \cdot 10^{-3}$
$ \sqrt{\theta}_{20} $	IP	$7.0 \cdot 10^{-4}$	$1.4 \cdot 10^{-3}$	$1.1 \cdot 10^{-4}$	$2.2 \cdot 10^{-8}$	$4.9 \cdot 10^{-3}$
$ \sqrt{\theta}_{21} $	LOANS	$1.2 \cdot 10^{-3}$	$2.5 \cdot 10^{-3}$	$1.5 \cdot 10^{-4}$	$2.1 \cdot 10^{-8}$	$8.5 \cdot 10^{-3}$
$ \sqrt{\theta}_{22} $	M3	0.027	0.024	0.023	$3.7 \cdot 10^{-7}$	0.086
$ \sqrt{\theta}_{23} $	CAR	$2.9 \cdot 10^{-3}$	$5.1 \cdot 10^{-3}$	$5.3 \cdot 10^{-4}$	$3.0 \cdot 10^{-8}$	0.018
$ \sqrt{\theta}_{24} $	OIL	$9.0 \cdot 10^{-4}$	$1.8 \cdot 10^{-3}$	$1.2 \cdot 10^{-4}$	$2.0 \cdot 10^{-8}$	$6.4 \cdot 10^{-3}$
$ \sqrt{\theta}_{25} $	ORDER	$1.3 \cdot 10^{-3}$	$2.8 \cdot 10^{-3}$	$1.7 \cdot 10^{-4}$	$2.4 \cdot 10^{-8}$	$9.5 \cdot 10^{-3}$
$ \sqrt{\theta}_{26} $	UNEMP	0.033	0.400	$8.5 \cdot 10^{-3}$	$5.6 \cdot 10^{-8}$	0.120
$ \sqrt{\theta}_{27} $	$D_{t,1}$	$2.6 \cdot 10^{-3}$	$4.9 \cdot 10^{-3}$	$3.7 \cdot 10^{-4}$	$3.0 \cdot 10^{-8}$	0.017
$ \sqrt{\theta}_{28} $	$D_{t,2}$	$3.9 \cdot 10^{-3}$	$6.8 \cdot 10^{-3}$	$5.9 \cdot 10^{-4}$	$3.2 \cdot 10^{-8}$	0.024
$ \sqrt{\theta}_{29} $	$D_{t,3}$	$4.0 \cdot 10^{-3}$	$7.4 \cdot 10^{-3}$	$5.8 \cdot 10^{-4}$	$3.1 \cdot 10^{-8}$	0.026
$ \sqrt{\theta}_{30} $	$D_{t,4}$	$2.3 \cdot 10^{-3}$	$4.5 \cdot 10^{-3}$	$3.0 \cdot 10^{-4}$	$2.7 \cdot 10^{-8}$	0.016
$ \sqrt{\theta}_{31} $	$D_{t,5}$	$2.4 \cdot 10^{-3}$	$4.6 \cdot 10^{-3}$	$3.4 \cdot 10^{-4}$	$2.8 \cdot 10^{-8}$	0.016
$ \sqrt{\theta}_{32} $	$D_{t,6}$	$1.9 \cdot 10^{-3}$	$3.9 \cdot 10^{-3}$	$2.5 \cdot 10^{-4}$	$2.4 \cdot 10^{-8}$	0.013
$ \sqrt{\theta}_{33} $	$D_{t,7}$	$2.6 \cdot 10^{-3}$	$5.1 \cdot 10^{-3}$	$3.5 \cdot 10^{-4}$	$2.6 \cdot 10^{-8}$	0.018
$ \sqrt{\theta}_{34} $	$D_{t,8}$	$2.0 \cdot 10^{-3}$	$4.0 \cdot 10^{-3}$	$2.2 \cdot 10^{-4}$	$2.3 \cdot 10^{-8}$	0.014
$ \sqrt{\theta}_{35} $	$D_{t,9}$	$2.3 \cdot 10^{-3}$	$4.5 \cdot 10^{-3}$	$3.4 \cdot 10^{-4}$	$3.0 \cdot 10^{-8}$	0.016
$ \sqrt{\theta}_{36} $	$D_{t,10}$	$2.2 \cdot 10^{-3}$	$4.4 \cdot 10^{-3}$	$2.6 \cdot 10^{-4}$	$2.4 \cdot 10^{-8}$	0.015
$ \sqrt{\theta}_{37} $	$D_{t,11}$	$3.2 \cdot 10^{-3}$	$5.7 \cdot 10^{-3}$	$5.1 \cdot 10^{-4}$	$2.9 \cdot 10^{-8}$	0.020
$\sigma^2$		0.011	$4.2 \cdot 10^{-3}$	0.010	$4.0 \cdot 10^{-3}$	0.020

Table A.3: ECB data. Posterior summary statistics for  $p(\beta_j|\mathbf{y})$  and  $p(\sqrt{\theta_j}|\mathbf{y})$  under the hierarchical double gamma prior with  $a^\tau \sim \mathcal{E}(10)$  and  $a^\xi \sim \mathcal{E}(10)$  for  $j = 1, \dots, 37$ .  $D_{t,k}$  is a monthly 0/1 dummy variable taking the value 1 for month  $k$  ( $k = 1, \dots, 11$ ) and 0 otherwise.

$i$	Symbol	Name	$i$	Symbol	Name
1	ADS	Adidas	16	FRE	Fresenius
2	ALV	Allianz	17	FME	Fresenius Medical Care
3	BAS	BASF	18	HEI	HeidelbergCement
4	BAYN	Bayer	19	HEN3	Henkel
5	BEI	Beiersdorf	20	IFX	Infineon Technologies
6	BMW	BMW	21	SDF	K + S
7	CBK	Commerzbank	22	LIN	Linde
8	CON	Continental	23	MRK	Merck
9	DAI	Daimler	24	MUV2	Munich Re
10	DBK	Deutsche Bank	25	RWE	RWE
11	DB1	Deutsche Börse	26	SAP	SAP
12	LHA	Deutsche Lufthansa	27	SIE	Siemens
13	DPW	Deutsche Post	28	TKA	ThyssenKrupp
14	DTE	Deutsche Telekom	29	VOW3	Volkswagen Group
15	EOAN	E.ON			

Table A.2: DAX data. Data description.

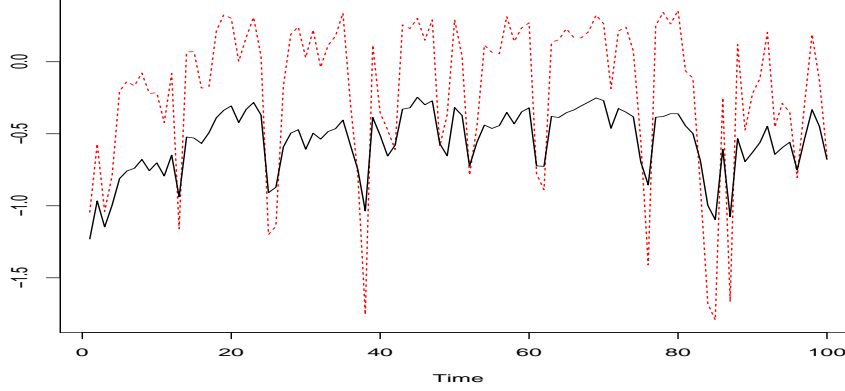


Figure A.2: ECB data. Comparing the conditionally optimal Kalman mixture approximation (full line) and the naive Gaussian mixture approximation (dashed line) of the log predictive density scores  $\text{LPDS}_t^*$  ( $t = t_0 + 1, \dots, t_0 + 100, t_0 = 90$ ) for the last 100 time points.

### A.3.2 Comparing approximations to the one-step ahead predictive density

For the inflation data discussed in Section 7.1, it is essential to use an accurate approximation method such as the conditionally optimal Kalman mixture approximation rather than the naive mixture approximation discussed in Section A.1.2.2 to approximate the one-step ahead predictive density  $p(y_t|\mathbf{y}^{t-1})$ . Since both approximations are finite mixtures of Gaussian distributions, the value of each mixture component pdf need to be calculated at the actually observed value  $y_t$  in order to derive the log predictive density score  $\text{LPDS}_t^*$ . Despite the high number of mixture components ( $M = 100,000$ ), the resulting approximations of  $\text{LPDS}_t^*$  turned out to differ substantially, see Figure A.2, where a comparison is provided for the hierarchical double gamma prior with  $a^\tau \sim \mathcal{E}(10)$  and  $a^\xi \sim \mathcal{E}(10)$ .

In Figure A.3 we compare a small subset of the mixture component densities  $p(y_t|\mathbf{y}^{t-1}, \boldsymbol{\vartheta})$  for both approximations of  $\text{LPDS}_t^*$  for a single point in time ( $t = 130$ ), where respectively  $\boldsymbol{\vartheta} = (\beta_t, \sigma_t^2)$  and  $\boldsymbol{\vartheta} = (\beta_1, \dots, \beta_d, \sqrt{\theta_1}, \dots, \sqrt{\theta_d}, \sigma_t^2)$ . The observed value  $y_t$  is indicated by a vertical line. Compared to the conditionally optimal Kalman mixture approximation, the mixture components of the naive approximation have a very small spread, typical of a high signal-to-noise ratio. A large number of zeros results from density evaluation and leads to a bias of the corresponding estimate of  $\text{LPDS}_t^*$  toward zero and, depending on the true value, the log predictive density score  $\text{LPDS}_t^*$  is over- or underrated.

For the DAX data analyzed in Section 7.2, the naive Gaussian mixture approximation yields identical estimated of  $\text{LPDS}_t^*$  for nearly all time point, see Figure A.4, mainly

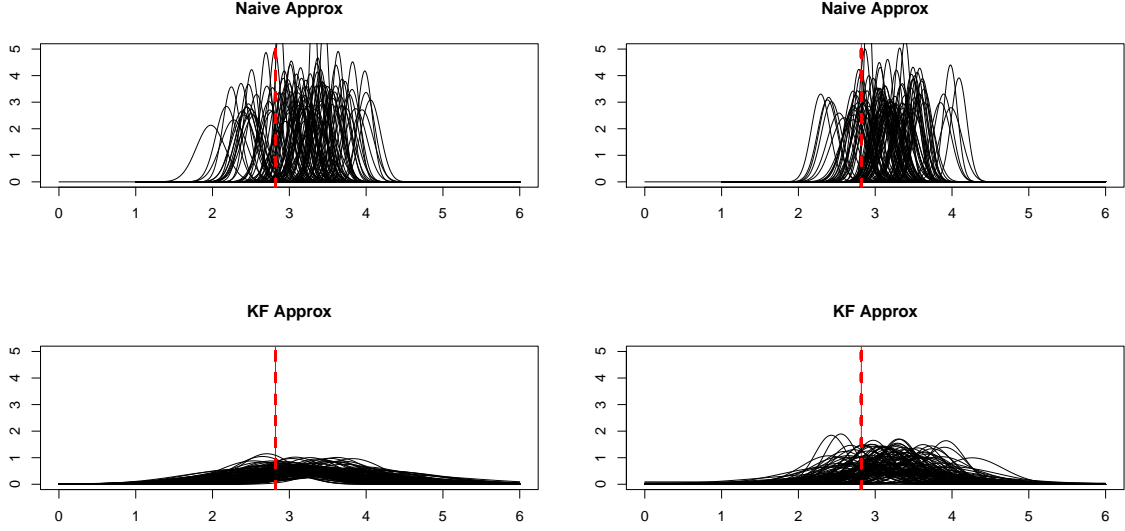


Figure A.3: ECB data. Illustration of the naive mixture approximation and the conditionally optimal Kalman mixture approximation for the predictive density  $p(y_t|y^{t-1})$  at  $t = 130$  for the hierarchical double gamma prior with  $a^\tau \sim \mathcal{E}(10)$  and  $a^\xi \sim \mathcal{E}(10)$  (left-hand side) and the hierarchical Bayesian Lasso prior (right-hand side). The observed value  $y_t$  is indicated by the vertical line. For both mixture approximations, 40 components densities  $p(y_t|\mathbf{y}^{t-1}, \boldsymbol{\vartheta}^{(m)})$  are plotted for randomly selected draws  $\boldsymbol{\vartheta}^{(m)}$  from the posterior  $p(\boldsymbol{\vartheta}|\mathbf{y}^{t-1})$ .

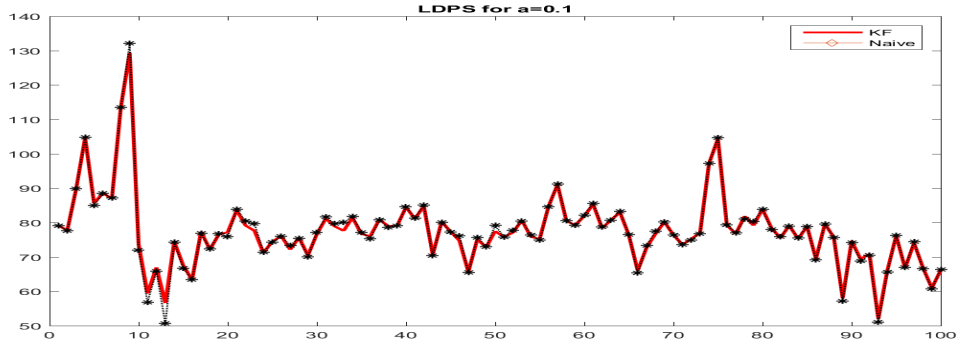


Figure A.4: DAX data. Comparing approximations of the overall log predictive densities scores  $\text{LPDS}_{t+1}^*$  for  $a^\tau = a^\xi = 0.1$  obtained from the optimal Kalman mixture approximation (full line) and the naive Gaussian mixture approximation (dashed line with  $\star$ ).

because the variance of all conditional mixture densities  $p(y_{i,t}|\mathbf{y}^{t-1}, \boldsymbol{\vartheta})$  is dominated by  $\sigma_{i,t}^2$  for both approximations due to the low signal-to-noise ratio.



## References

- Belmonte, M. A. G., Koop, G., and Korobolis, D. (2014). Hierarchical shrinkage in time-varying parameter models. *Journal of Forecasting*, 33:80–94.
- Carter, C. K. and Kohn, R. (1994). On Gibbs sampling for state space models. *Biometrika*, 81:541–553.
- Cogley, T., Morozov, S., and Sargent, T. (2005). Bayesian fan charts for U.K. inflation: Forecasting and sources of uncertainty in an evolving monetary system. *Journal of Economic Dynamics and Control*, 16:1893–1925.
- Frühwirth-Schnatter, S. (1992). Approximate predictive integrals for dynamic generalized linear models. In Fahrmeir, L., Francis, B., Gilchrist, R., and Tutz, G., editors, *Advances in GLIM and Statistical Modelling*, number 78 in Lecture Notes in Statistics, pages 123–151. Springer, New York.
- Frühwirth-Schnatter, S. (1994). Data augmentation and dynamic linear models. *Journal of Time Series Analysis*, 15:183–202.
- Hörmann, W. and Leydold, J. (2014). Generating generalized inverse gaussian random variates. *Statistics and Computing*, 24:547–557.
- Hörmann, W. and Leydold, J. (2015). GIGrvg: Random variate generator for the GIG distribution. R package version 0.4, url: <http://CRAN.R-project.org/package=GIGrvg>.
- Kastner, G. and Frühwirth-Schnatter, S. (2014). Ancillarity-sufficiency interweaving strategy (ASIS) for boosting MCMC estimation of stochastic volatility models. *Computational Statistics and Data Analysis*, 76:408–423.
- McCausland, W. J., Miller, S., and Pelletier, D. (2011). Simulation smoothing for state space models: A computational efficiency analysis. *Computational Statistics and Data Analysis*, 55:199–212.
- Rue, H. and Held, L. (2005). *Gaussian Markov Random Fields: Theory and Applications*, volume 104 of *Monographs on Statistics and Applied Probability*. Chapman & Hall/CRC, London.